이학박사 학위논문

Development of novel cell-internalizing peptides using in vivo intermolecular conjugation as an avenue for enhancing the effect of anti-angiogenic therapy on tumors

종양 신생혈관 억제 치료 효과 증진을 위한
체내 분자 간 결합을 이용한 세포 내재화 펩티드 개발

2019년 8월

서울대학교 융합과학기술대학원
융합과학부 방사선융합의생명전공
최 지 영

Development of novel cell-internalizing peptides using in vivo intermolecular conjugation as an avenue for enhancing the effect of anti-angiogenic therapy on tumors

지도교수 김 상 은

이 논문을 이학박사 학위논문으로 제출함

2019년 7월

서울대학교 융합과학기술대학원

융합과학부 방사선융합의생명전공

최 지 영

최지영의 이학박사 학위논문을 인준함

2019년 7월

위 원 장	김 재 용	(인)
부 위 원 장	김 상 은	(인)
위 원	윤 혜 원	(인)
위 원	이 병 철	(인)
위 원	이 은 성	(인)

Abstract

Development of novel cell-internalizing peptides using in vivo intermolecular conjugation as an avenue for enhancing the effect of anti-angiogenic therapy on tumors

Ji Young Choi

Program in Biomedical Radiation Sciences

Graduate School of Convergence Science and Technology

Seoul National University

Targeted cancer therapy (TCT) is distinct from other medical modalities, such as traditional chemotherapy, surgery, and external radiation therapy, as it targets cancer cells expressing specific biomarkers. Recently, there have been several approaches for TCT such as targeted chemotherapy, radionuclide therapy, and photodynamic

therapy which are preferring to minimize normal cell damage against tumor cells. As an ideal agent for TCT, small molecule, peptide or protein has to contain high binding property to tumor-specific biomarker, low non-selective distribution in normal organs, and long uptake in tumor cells including cell-internalization. In this study, we designed an in vivo intermolecular click reaction, which is named as 'Duet Bioorthogonal Clasp (DBC)', between different peptides that had situated in same tumor-specific receptors, after the respective injecting in tumor animal model. This strategy means that the strong and tight receptor cluster via in vivo click reaction induces endocytosis of the mixture of receptors and peptides into tumor cells and then results significant improvement of the tumor uptake of peptide as well as therapeutic effect. Therefore, integrin $\alpha_v\beta_3$ receptor and cyclic RGD analog peptide are selected as a tumor-specific biomarker related with angiogenesis and a molecule with high binding affinity to integrins, respectively. In addition, the RGD analog peptide was prepared to measure its biodistribution as well as single photon emission computed tomography (SPECT) imaging study through the corresponding of a radioisotope (^{123}I or ^{125}I).

The result showed that the two different RGD peptides bound to the integrin $\alpha_v\beta_3$ receptors were significantly moved to into tumor cells, by using Fluorescence Resonance Energy Transfer (FRET) microscopy. In the SPECT imaging experiment using the radioiodine-labeled RGD peptide, DBC maintained 81% of tumor uptake 2 h post-injection compared to its initial uptake (vs. control tumor uptake was remained 39% at the same time point). After 24 h

postinjection, 60% of tumor uptake still observed.

In conclusion, DBC is demonstrated that it can generate the strong cluster between integrin receptors near cancer cells which induce cancer cell internalization. These results suggest that this methode can pave the way to various successful application of a therapeutic molecules or radioisotope capable of cell-internalization for TCTs.

Keywords : targeted cancer therapy, internalization, angiogenesis, RGD peptides, cluster

Student Number : 2014-30819

CONTENTS

FIGURE LEGENDS

TABLES LEGENDS

INTRODUCTION

1. Targeted cancer therapies (TCTs)

Cancer remains the leading cause of death worldwide for decades, treatment modalities for cancer has included surgery, external radiation therapy and, chemotherapy [1,2]. Chemotherapy uses anticancer drugs that target rapidly dividing cells, including but not exclusively cancer cells. Because they are distributed throughout the body and not localized to the cancer cells, these drugs affecting the normal cells as well [3]. Most of the chemotherapeutic agents, which have the lack of specific targets for cancer treatment, lead to increase toxicities of normal tissues so that many patients experience the classic symptoms, such as alopecia, gastrointestinal symptoms, and myelosuppression [4,5]. Therefore, a dramatic shift has taken place in cancer therapy from chemotherapy to targeted therapy [6]. The term 'targeted therapy' refers to a new generation of cancer therapy that interferes with a biomarker or specific target that is related to tumor growth or progression [7]. These strategies are aimed at preferentially killing cancer cells without exhibiting any significant toxic effect on normal cells[8]. The targeted therapy includes targeted radionuclide therapy, photodynamictherapy and immunotherapy [9]. In particular, targeted therapy involved the use ligands that show high-affinity for a cancer biomarker and directly interact with the cancer cells, functioning as carriers [10]. The molecules for targeted therapy consist of target specific ligands including small molecules, peptides and antibodies [11]. Moreover, high selectivity, stability and ability for internalization

of ligands are important for targeted therapy.

2. Tumor-induced angiogenesis

Biomarkers capable of improving therapeutic response and targeting cancer play a key role in the targeted therapy [12]. Because cancer biomarkers are substances or processes that indicate the presence of cancer in the body, they can be associated with "hallmarks of cancer" [13]. Hanahan and Weinberg have categorized hallmarks of cancer, which include unlimited proliferative potential, environmental independence for growth, evasion of apoptosis, angiogenesis, invasion ,and metastasis to different parts of the body (**Figure 1**) [14]. Based on an understanding of proposed hallmarks of cancer, this study focused on tumor induced-angiogenesis and its biomarker.

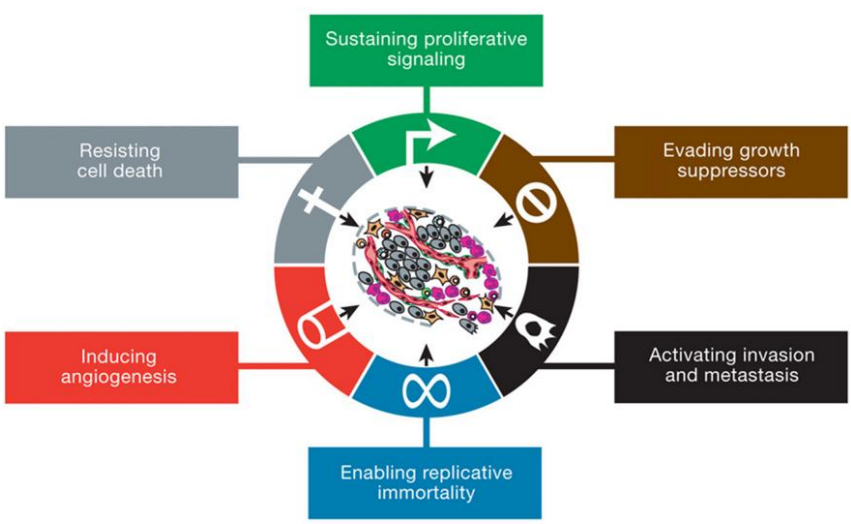

Figure 1. The hallmark of cancer [14]

Angiogenesis is a process of forming new blood vessels from existing ones and an essential mechanism to supply sufficient oxygen and nutrients for tumor growth, invasion and metastasis [15]. Tumor-induced angiogenesis is a complex events related with various growth factors, cellular receptors and adhesion molecules [16]. It is primarily regulated by vascular endothelial growth factor and cell adhesion receptor integrins [17]. Integrins, comprising α and β transmembrane subunits, interact with activated endothelial cells [18,19]. Particularly, integrin $\alpha_v\beta_3$ is overexpressed by activated endothelial cells during tumor growth and are located at the surface of angiogenic blood vessels on various tumors such as ovarian cancer, glioblastoma, breast cancer and melanoma (**Figure 2**) [20,21]. The high expression of integrin $\alpha_v\beta_3$ on new blood vessels for various tumor promises to be promising biomarker for targeted therapy [22,23].

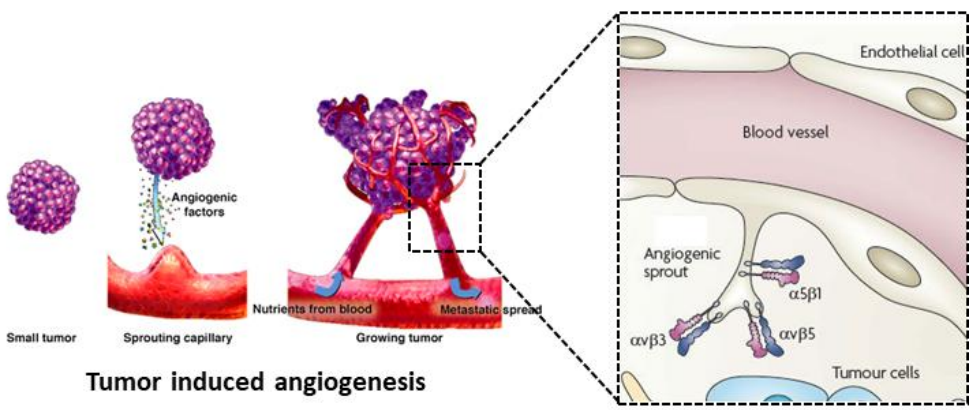

Figure 2. Tumor induced angiogenesis [20,21]

3. Integrin-binding peptide for tumor imaging

The tripeptide sequence of arginine-glycine-aspartic acid (RGD) derivative is well known for ligand for binding integrin $\alpha_v\beta_3$ which plays a key role in modulating tumor angiogenesis [24,25]. While linear RGD peptide are highly susceptible to chemical decomposition, numerous studies have reported that the cyclic RGD peptide are highly stable in vivo and show high affinity for stability for targeting receptors (**Figure 3**) [26]. Because cyclic peptides has rigidity by cyclization, it is generally more stable and specific to integrin $\alpha_v\beta_3$ than linear [27]. In particular, cyclic peptide c(RGDfK), obtained from cyclization of a linear RGD pentapeptide containing an unnatural D-phenylalaine (D-Phe), is commonly used as ligand [28,29].

Multimeric cyclic RGD peptides, which have multiple cyclic RGD peptides, have been reported to show enhanced in vitro binding affinity for integrin $\alpha_v\beta_3$ on cancer cells (**Table 1**) [30,31].

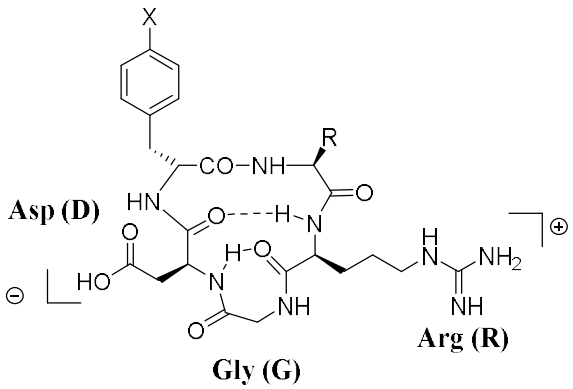

Figure 3. Structure of cyclic RGD peptides

Table 1. IC_{50} values of reported multimeric cyclic RGD peptides [30]

Compound	IC_{50} (nM)
c(RGDyK)	458 ± 45
HYNIC-P-RGD	452 ± 11
HYNIC-RGD2	112 ± 21
HYNIC-P-RGD2	84 ± 7
HYNIC-RGD4	7 ± 2

The high cell-binding affinity of multimeric RGD peptide could be explained by endocytosis of ligand-bound integrin $\alpha_v\beta_3$ [32]. Interactions between integrin $\alpha_v\beta_3$ and RGD peptide could provide higher cellular uptake through the integrin-dependent endocytosis pathway [33].

Endocytosis of integrin means an internalization of receptors from the plasma into an internal membrane [34]. Generally, there are two types of pathways associated with the internalization of integrin [35]. One is a clathrin-mediated endocytosis and the other is a clathrin-independent endocytosis [36]. Integrin $\alpha_v\beta_3$ primarily internalized via clathrin-dependent endocytosis, which is initiated from clustering of integrin $\alpha_v\beta_3$ [37].

After the RGD peptide binds to its receptor, ligand-bound integrin begin to form a cluster [38]. The clusters of integrin $\alpha_v\beta_3$ at ligand binding sites stabilized by cytoplasmic adhesion proteins that crosslink the integrin cytoplasmic tails plus connect the clusters to the cell cytoskeleton (**Figure 4**) [39]. This stabilized state, which is gathering of integrins, can accelerate process of endocytosis. Therefore, the clusters appear to be very important elements in many cellular processes and can be considered as a critical functional module. Besides, the clustering of receptors has obvious the advantage for the increased endocytosis of ligand-bound integrin $\alpha_v\beta_3$ [40].

Several studies have proved this process that multimeric RGD peptides were internalized into cancer cell by receptor clustering and subsequent endocytosis [41,42]. From in vitro cell assay, monomeric cyclic RGD peptides were internalized independent of integrin $\alpha_v\beta_3$, whereas multimeric cyclic RGD peptides were internalized with their receptor via clustering of integrins [41,42]. Multimeric cyclic RGD peptides more strongly bound to integrin $\alpha_v\beta_3$ and more efficiently co-internalized with the receptor via clustering of integrins [41,42].

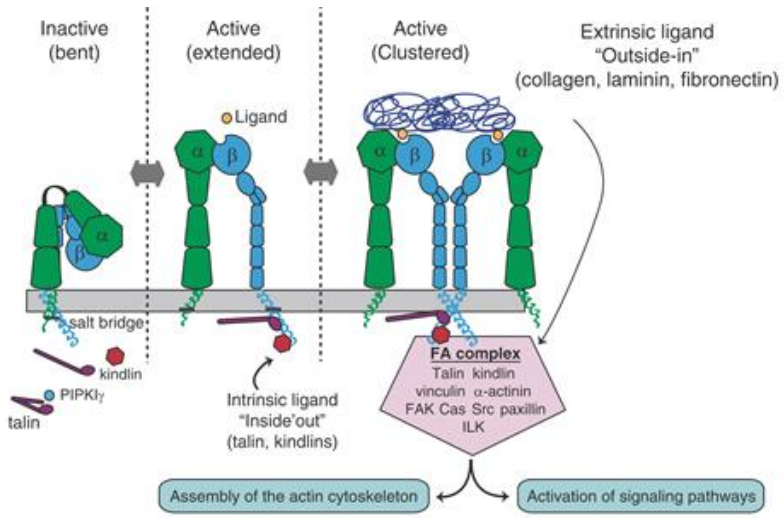

Figure 4. Cluster and endocytosis of ligand-bound intergrin $\alpha_v\beta_3$ [39].

Although multimeric RGD peptides had a significantly high cell-binding affinity for tumor, some in vivo studies shown multimeric concept has rapid excretion on tumor [43,44]. Wu and colleagues synthesized ^{18}F-FPRGD2 (cyclic RGD dimer) and ^{18}F-FPRGD4 (cyclic RGD tetramer) and compared their the tumor targeting efficacy and in vivo kinetics [43]. Results of in vivo micro PET study showed that the tumor uptake of ^{18}F-FPRGD4 was higher than that of ^{18}F-FPRGD2 at all time points in the U87-MG xenograft model but the tumor uptake of both ligands reduced to half of the initial uptake after 2 h [43]. Lee et al. synthesized ^{99m}Tc-IDA-D-[c(RGDfK)]$_2$ as radiotracer for SPECT/CT imaging. This ligand has high uptake and selectivity for several tumors and diseases related with infarction. However, it also has short half-life (122.7 min) for tumor uptake [44].

Furthermore, studies that applied multimeric cyclic RGD peptide to targeted cancer therapy, suggested that fast washout on tumor affected the efficacy of therapy [45,46].

Janssen and co-workers firstly investigated the effects of integrin $\alpha_v\beta_3$ targeted radionuclide therapy with ^{90}Y-DOTA-E-[c(RGDfK)]$_2$ in an ovarian carcinoma-bearing mouse model [41]. Tumor growth was inhibited by a single injection of ^{90}Y-DOTA-E-[c(RGDfK)]$_2$ [45]. However, considerable uptake in non-target organs such as spleen, liver, and kidney was observed, and multiple injections and high dose were required to enhance the therapeutic efficacy [45]. In the following study, both ^{90}Y-DOTA-RGD4 and ^{90}Y-DOTA-3PRGD2 induced inhibition of tumor growth in the U87-MG-bearing mouse model [46]. However, high dose or multiple injections of ligands were still required to achieve maximum therapeutic efficacy due to rapid washout of tumor uptake [46].

One of the reasons for a fast washout at the tumor site is that multimeric cyclic RGD peptides could not simultaneously bind integrin $\alpha_v\beta_3$ under in vivo environments (**Figure 5**). There are various factors such as blood pressure, the density of integrin $\alpha_v\beta_3$ and pH that influence the ligand-receptor interaction in the cancer microenvironments. If multimeric cyclic RGD peptides were difficult to bind to multiple integrin $\alpha_v\beta_3$ simultaneously, it would not show the advantages of multimeric effect, such as enhanced binding affinity and retention on cancer [47,48]. Moreover, receptor clustering and endocytosis of ligand-bound integrin would not be favored as well.

Therefore, the new strategy is required to ensure strong binding with integrin $\alpha_v\beta_3$ and clustering under in vivo environments. This study designed the method, which induces in vivo clustering of intergrin $\alpha_v\beta_3$ by using intermolecular conjugation of cyclic RGD peptides.

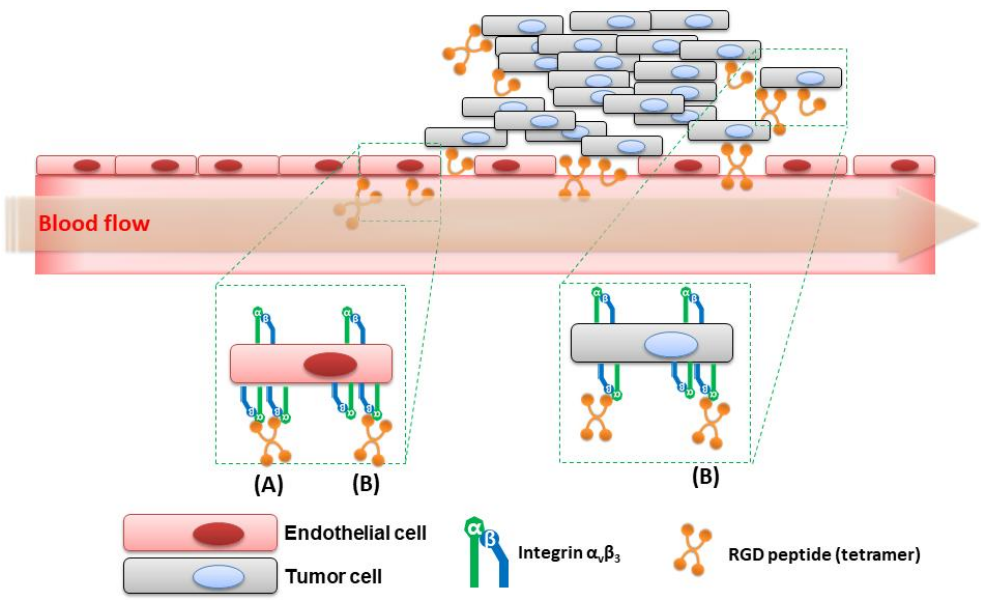

Figure 5. Schematic illustration of the interactions between mutimeric cyclic RGD peptide and integrin $\alpha_v\beta_3$. (A) The multimeric cyclic RGD peptides bind integrin $\alpha_v\beta_3$ at the same time. The process of clustering and endocytosis of ligand-bound receptor could start from this state. (B) The two RGD motifs, which is named cyclic RGD dimer is not enough for simultaneous integrin $\alpha_v\beta_3$ binding.

4. In vivo intermolecular conjugation

For in vivo intermolecular conjugation, click reaction was considered in this study. Click reaction, first described by Kolb, involves copper-catalysed formation of 1,2,3-triazole by [2+3] cycloaddition of terminal alkynes and azides [49,50]. Although this method is an attractive synthetic process because of its convenient, cytotoxicity of copper is an obstacle for its in vivo application [51,52].

In the following study, the Bertozzi group developed the copper-free click reactions, which was referred to as strain promoted azide-alkyne cycloaddition (SPAAC) of azide-azadibenzocyclooctyne (ADIBO) [53,54]. Recently, Inverse Electron Demand Diels–Alder (IEDDA) of tetrazine-trans-cyclooctene (TCO) with fast kinetics was reported (**Figure 6**) [55]. The copper-free click reaction carried out under aqueous condition at room temperature and is completed a short period [56]. Therefore, many groups adapted copper-free click reaction to in vivo system because of its high stability, reactivity ,and utility [57]. For these reasons, copper-free click reaction were used for in vivo intermolecular conjugation in this study.

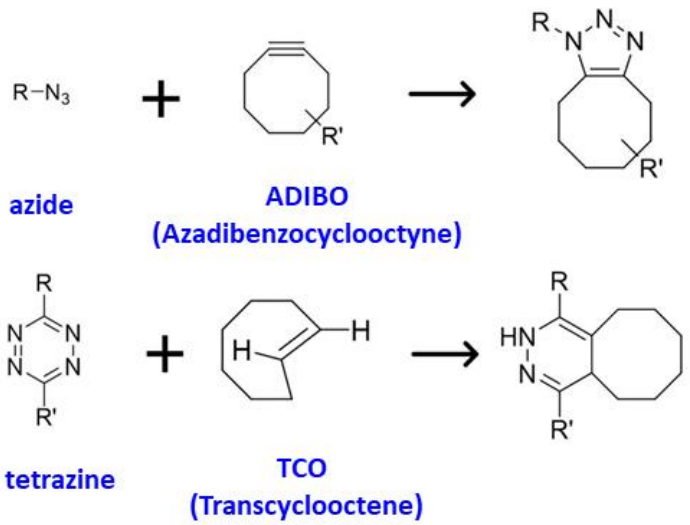

Figure 6. Copper free Click reaction.

5. Aim of this study

This study was aimed at developing a strategy to ensure that the ligands are strongly bound to the receptors and that the ligand bound receptors form clusters. For this, in situ intermolecular click reaction between different RGD peptides that are bound to their tumor-specific receptors, resulting in the formation a '*Dual Bioorthogonal Clasp* (DBC)' was designed. This was envisaged to strengthen the ligand-receptor interactions and induce endocytosis of ligand-bound integrin $\alpha_v\beta_3$ into tumor cells to enhance tumor uptake of the peptide as well as increase the retention time at the cancer site (**Figure 7**).

For this method, two different cyclic RGD peptides containing click moiety for intermolecular conjugation were designed as integrin binding ligands. In addition, the radiolabeled RGD peptide was prepared to measure in vivo kinetics by single photon emission computed tomography (SPECT) imaging using the radioisotope ^{123}I or ^{125}I [APPENDIX 1]. The internalization of integrin $\alpha_v\beta_3$ receptors on tumor cells was evaluated by fluorescence resonance energy transfer (FRET) microscopy [APPENDIX 2].

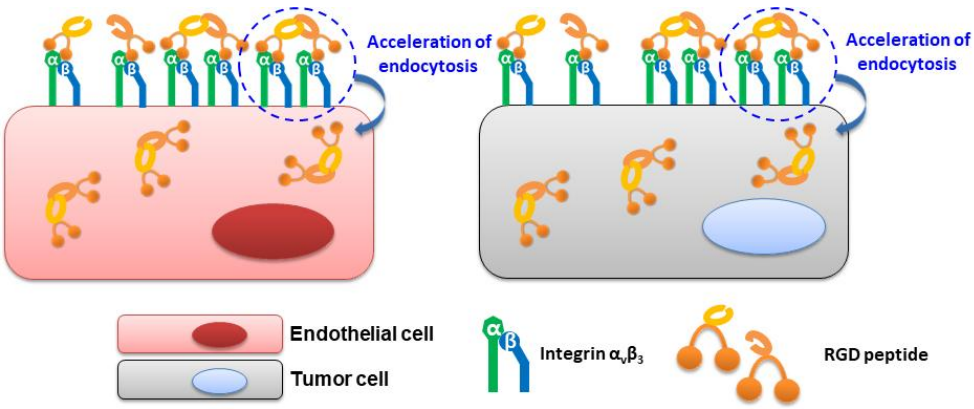

Figure 7. Schematic illustration of 'Dual Bioorthogonal Clasp (DBC)' in this study

MATERIALS & METHOD

1. General experimental section

All commercial reagents and solvents were used without further purification unless otherwise specified and were purchased from Sigma-Aldrich, Tokyo Chemical Industry Co. (TCI), Alfa Aesar and Futurechem. Electrospray mass spectrometry (ESI-MS) was performed on a LC/MS spectrometer (Agilent 6130 Series). Radio-TLC on Merck F254 silica plate was analyzed by using a Bioscan radio-TLC scanner. All radioactivities were measured using a VDC-505 activity calibrator from Veenstra Instruments. [^{123}I]NaI was purchased from Korea Institute of Radiological and Medical Sciences (KIRAMS). The purification by HPLC was carried out on Agilent equipped with a UV detector (wavelength set at 214 or 254 nm) and a gamma-ray detector (Bioscan) using a semi-preparative column (Waters, Xterra RP-18, 10 μm, 10 × 250 mm). All solvents (J. T. Baker, U. S.) were used for HPLC purification after membrane filtering (Whatman, 0.22 μm). The column was eluted with a solvent mixture of acetonitrile and water containing 0.1% formic acid. The HPLC eluent started with 5% acetonitrile contained 0.1% formic acid and the ratio was increased from 40% acetonitrile to 60% containing 0.1% formic acid over 30 min at a flow rate of 3 mL/min.

Cell culture: U87-MG (human gliblastoma) was grown in Dulbecco's Modified Eagle's Medium (DMEM). A549 (human lung adenocarcinoma) was maintained in RPMI1640. All media were 10% fetal bovine serum (FBS) and 1% antibiotics (10,000 unit/mL of penicillin and 10,000 μg/mL of streptomycin) / antimycotics (25 μg/mL of Fungizone®). Cultures were maintained at 37 ℃ in a humidified 95% air and 5% CO_2 atmosphere [44].

U87-MG tumor xenografted mouse model: All animal experiments were conducted under a protocol approved by SNUBH Institutional Animal Care and Use Committee (IACUC). BLAB/c athymic mice (OrientBio, male, 6-7 weeks) were used in all experiments. U87-MG cells were cultured for 2–3 days, without changing the media, and harvested with 0.25% trypsin-EDTA solution. 1×10^7 U87-MG cells in 100 μL of PBS (pH 7.4) were injected subcutaneously in the right thigh of each mouse. Ex vivo biodistribution and in vivo animal SPECT/CT imaging studies conducted when the each tumor reached a long diameter of 1 cm at 2-3 weeks after implanting of tumor cells in nude mice.

2. Synthesis of RGD peptides

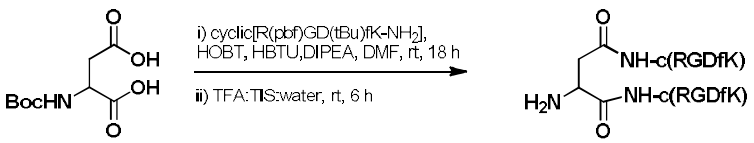

1 (NH_2-D-[c(RGDfK)]$_2$, 59%)

NH_2-D-[c(RGDfK)]$_2$ (1)

A solution of *N*-(*tert*-butoxycarbonyl)-L-aspartic acid (13 mg, 0.06 mmol), HOBT (32 mg, 0.24 mmol), HBTU (91 mg, 0.24 mmol) in DMF (2 mL) was added a mixture of c(RGDfK)-NH_2 (200 mg, 0.20 mol) and DIEA (83 μL, 0.48 mmol) in DMF (2 mL). The mixture was stirred at room temperature for 18 h. After concentration under reduced pressure, the crude mixture was purified with flash column chromatography (CH_2Cl_2:MeOH, v/v = 90:10). The resulting solution was dried under reduced pressure, BocNH-D-[c(RGDfK)]$_2$ (80 mg, 66%) was obtained as pale yellow semi-solid: MS (ESI) *m/z* 2020.1 $(M + H)^+$, 1010.5 $(M + 2H)^{2+}$

In order to removed the Boc group, A obtained BocNH-D-[c(RGDfK)]$_2$ (70 mg, 0.03 mmol) was treated with 4 mL of solution mixture with trifluoroacetic acid, triisopropylsilane and distilled water (v/v/v = 95 : 5 : 5). The solution was stirred at room temperature for 18 h. The solvent was removed under reduced pressure. The mixture was dissolved with methanol (2 mL) and added

with excess diethyl ether (20 mL), then white solid appeared. The solid was filtered, washed with diethyl ether and dried in vacuum, it gave NH_2-D-[c(RGDfK)]$_2$, (**1**, 35 mg, 89%) as pale yellow solid: MS (ESI) *m/z* 1304.6 $(M + H)^+$, 652.5 $(M + 2H)^{2+}$

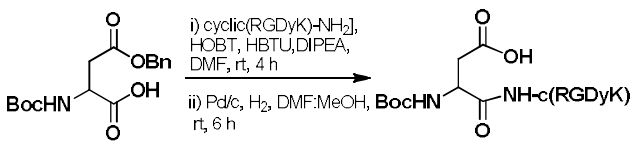

2 (65%)

BocNH-D-[c(RGDyK)]-COOH (**2**)

A solution of *N*-(*tert*-butoxycarbonyl)-L-aspartic acid 4-benzyl ester (50 mg, 0.15 mmol), HOBT (42 mg, 0.31 mmol), HBTU (118 mg, 0.31 mmol) in DMF (3 mL) was added to a mixture of c(RGDyK)-NH_2 (200 mg, 0.20 mmol) and DIEA (81 μL, 0.46 mmol) in DMF (3 mL). The mixture was stirred at room temperature for 4 h. The solvent was removed and dissolved with methanol (6 mL) then added excess diethyl ether (50 mL) to get the solid. The solid was filtered and washed with ether. The resulting solid was dissolved in a solvent mixture of water and CH_3CH (v/v = 95/5) and separated by a semi-preparative HPLC system. The expected product was collected at 27.1 min. After the resulting solution was dried under reduced pressure, it gave BocNH-D-[c(RGDyK)]-COOBn (100 mg, 72%) as pale yellow solid: MS (ESI) *m/z* 925.10 $(M + H)^+$

A obtained BocNH-D-[c(RGDyK)]-COOBn (100 mg, 0.11 mmol)

was dissolved in MeOH/DMF (v/v = 90/10, 5 mL) and treated with Pd/C (34 mg, 0.03 mmol). The mixture was stirred under H_2 gas at room temperature for 18 h. The resulting solution was filtered on celite and the filtrate was concentrated under reduced pressure. The solid was dissolved with methanol (6 mL) and added with excess diethyl ether (50 mL) to gain solid. The solid was filtered and washed with diethyl ether then dried in vacuo. The desired BocNH-D-[c(RGDyK)]-COOH (**2**, 82 mg, 90%) was obtained as pale yellow solid: MS (ESI) *m/z* 835.20 $(M + H)^+$

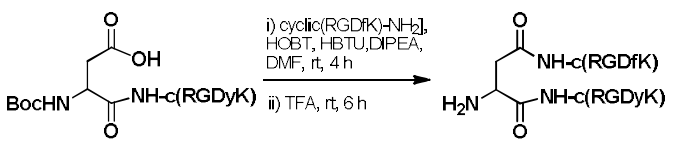

2 (65%) 3 (NH_2-D-[c(RGDfK)]-[c(RGDyK], 56%)

NH_2-D-[c(RGDyK)]-[c(RGDfK)] (**3**)

A solution of compound **2** (80 mg, 0.09 mmol), HOBT (26 mg, 0.19 mmol), HBTU (72 mg, 0.19 mmol) in DMF (2 mL) was added with a mixture of c(RGDfK)-NH_2 (69 mg, 0. 11 mmol) and DIEA (48 μL, 0.28 mmol) in DMF (2 mL). The mixture was stirred at room temperature for 4 h. The solvent was removed and dissolved with methanol (5 mL) added excess diethyl ether (30 mL) to get the solid. The solid was filtered and washed with ether then dissolved in a solvent mixture of water and CH_3CH (v/v = 95/5). The solution was separated by a semi-preparative HPLC system and the expected

product was collected at 25.1 min. After the resulting solution was dried under reduced pressure, it gave BocNH-D-c(RGDyK)-c(RGDfK**)** (79 mg, 62%) as pale yellow solid: MS (ESI) *m/z* 1420.6 $(M + H)^+$, 710.5 $(M + 2H)^{2+}$

A obtained BocNH-D-c(RGDyK)-c(RGDfK) (70 mg, 0.04 mmol) was dissolved in TFA/distilled water (v/v = 95/5, 2 mL) and stirred at room temperature for 4 h. The solvent was removed under reduced pressure and dissolved with methanol then added excess diethyl ether to get white solid. The solid was filtered and washed with diethyl ether. After the solid was dried in vacuum, it gave compound NH_2-D-[c(RGDyK)]-[c(RGDfK)], (**3**, 47 mg, 90%) as pale yellow solid: MS (ESI) *m/z* 1320.6 (M + H)+, 660.5 $(M + 2H)^{2+}$

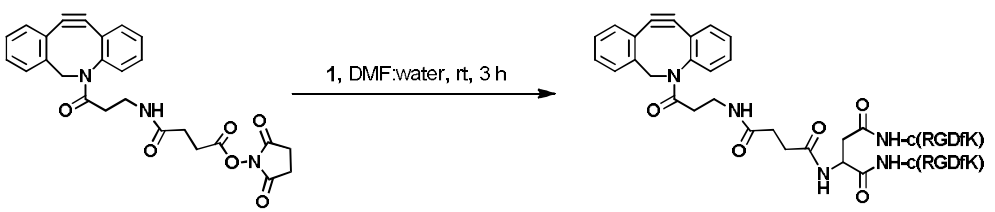

4 (ADIBO-D-[c(RGDfK)]$_2$, 60%

ADIBO-D-[c(RGDfK)]$_2$ (4)

The compound **1** (30 mg, 0.02 mmol) was dissolved in 2 mL of a solution mixture with DMF and water (v/v = 1/1) in a vial and added with azadibenzocyclooctyne-*N*-hydroxysuccinimidyl ester (ADIBO analog, 42 mg, 0.09 mmol). The mixture was stirred at room temperature for 3 h. The solution was diluted with water. The

solution was separated by a semi-preparative HPLC system. The expected product (ADIBO-D-[c(RGDfK)]$_2$, **4**) was collected at 25.4 min. After the resulting solution was dried under reduced pressure, it gave compound **7** (20 mg, 60%) as white solid: MS (ESI) *m/z* 1662.2 $(M + H)^+$, 831.5 $(M + 2H)^{2+}$

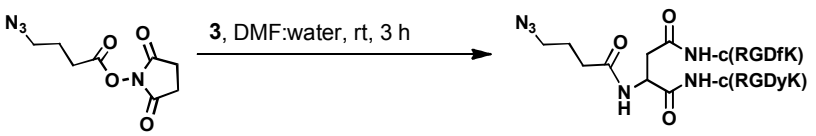

5, N_3-butyl-D-[c(RGDfK)]-[c(RGDyK)], 60%

N_3-butyl-D-[c(RGDyK)]-[c(RGDfK)] (5)

The compound **3** (40 mg, 0.03 mmol) was dissolved in 2 mL of solvent mixture with DMF and water (v/v = 1/1) in a vial and added succinimidyl 4-azidobutyrate (16 mg, 0.07 mmol). After the mixture was stirred at room temperature for 3 h, the solution was diluted with water and followed by sby a semi-preparative HPLC purification. The desired N_3-butyl-D-[c(RGDyK)]-[c(RGDfK)] (**5**) was collected at 21.1 min. After the resulting solution was dried under reduced pressure, it gave compound **4** (26 mg, 60%) as white solid: MS (ESI) *m/z* 1431.6 $(M + H)^+$, 716.3 $(M + 2H)^{2+}$

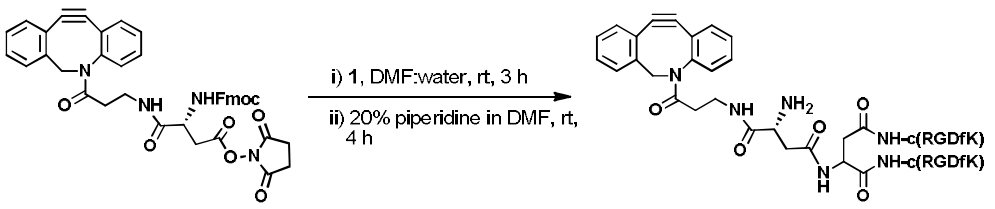

6, ADIBO-D-NH_2-D-[c(RGDfK)]$_2$, 62%

ADIBO-D-(NH_2)-D-[c(RGDfK)]$_2$ (6)

The compound **1** (40 mg, 0.03 mmol) was dissolved in DMF/DW (v/v = 1/1, 1 mL) in vial and added ADIBO-Asp(Fmoc)-NHS (42 mg, 0.06 mmol). The mixture was stirred at room temperature for 3 h. After removing the solvent, the solution was diluted with water and separated by a semi-preparative HPLC system. The desired compound was collected at 27.2 min. The solid was added 20% piperidine in DMF and was stirred for 4 h at room temperature. The solvent was removed under reduced pressure and dissolved with methanol then added excess diethyl ether to get white solid. The solid was filtered and washed with diethyl ether. After the resulting solution was dried under reduced pressure, it gave ADIBO-D-NH_2-D-[c(RGDfK)]$_2$, (**6**, 26 mg, 62%) as white solid: MS (ESI) *m/z* 1677.8 $(M + H)^+$, 834.4 $(M + 2H)^{2+}$.

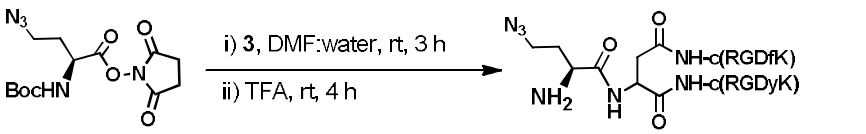

7, N_3-K-D-[c(RGDfK)]-[c(RGDyK)], 61%

N_3-K-D-[c(RGDfK)]-[c(RGDyK)] (**7**)

The compound **3** (30 mg, 0.02 mmol) was dissolved in 1 mL of solvent mixture with DMF and water (v/v = 1/1) in a vial and added to N_3-Lys(Boc)-NHS (17 mg, 0.05 mmol). The mixture was stirred at room temperature for 3 h. After removing solvent, the reaction mixture was diluted with water and separated by a semi-preparative HPLC system. The desired compound was collected at 23.1 min. The solid was treated with TFA and then was stirred for 4 h at room temperature. After removing TFA under reduced pressure, the reaction mixture dissolved with methanol then added excess diethyl ether to get white solid. After the resulting solution was dried under reduced pressure, it gave N_3-K-D-[c(RGDfK)]-[c(RGDyK)] (**7,** 26 mg, 61%) as white solid: MS (ESI) *m/z* 1474.6 $(M + H)^+$, 737.5 $(M + 2H)^{2+}$

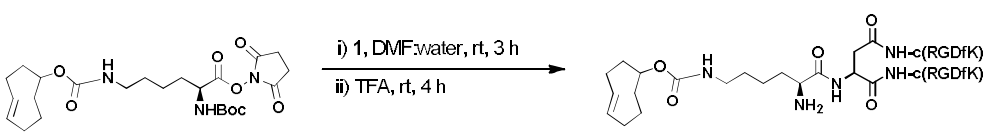

8 (TCO-K-D-[c(RGDfK)]$_2$, 44%)

TCO-K-NH_2-D-[c(RGDfK)]$_2$ (8)

The compound **1** (40 mg, 0.03 mmol) was dissolved in 1 mL of

solvent mixture with DMF and water (v/v = 1/1) in vial and added TCO-Lys(Boc)-NHS (34 mg, 0.07 mmol). The mixture was stirred at room temperature for 3 h. After removing solvent, the reaction mixture was diluted with water and separated by a semi-preparative HPLC system. The desired compound was collected at 26.6 min. The solid was treated with TFA and then was stirred for 4 h at room temperature. After removing TFA under reduced pressure, the reaction mixture dissolved with methanol then added excess diethyl ether to get white solid. After the resulting solution was dried under reduced pressure, it gave TCO-K-NH_2-D-[c(RGDfK)]$_2$ (**8,** 21 mg, 44%) as white solid: MS (ESI) *m/z* 1583.8 $(M + H)^+$, 192.2 $(M + 2H)^{2+}$.

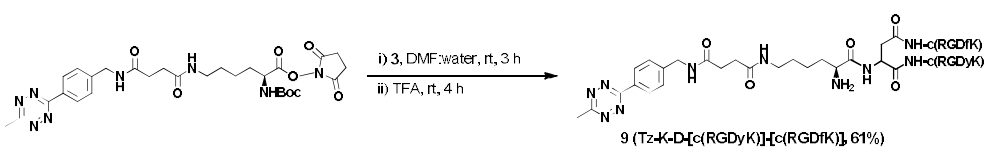

Tz-K-D-[c(RGDfK)]-[c(RGDyK)] (9)

The compound **3** (20 mg, 0.03 mmol) was dissolved in 1 mL of solvent mixture with DMF and water (v/v = 1/1) in a vial and added to tetrazine-Lys(Boc)-NHS (43 mg, 0.07 mmol). The mixture was stirred at room temperature for 3 h. After removing solvent, the reaction mixture was diluted with water and separated by a semi-preparative HPLC system. The desired compound was collected at 24.8 min. The solid was treated with TFA and then was stirred for 4 h at room temperature. After removing TFA under reduced pressure,

the reaction mixture dissolved with methanol then added excess diethyl ether to get white solid. After the resulting solution was dried under reduced pressure, it gave product Tz-K-D-[c(RGDfK)]-[c(RGDyK)] (**9,** 26 mg, 61%) as white solid: MS (ESI) *m/z* 1730.8 $(M + H)^+$, 866.5 $(M + 2H)^{2+}$

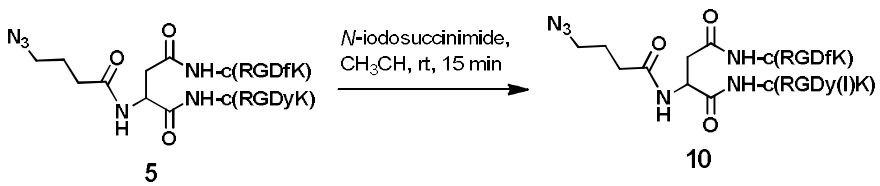

5 10

N_3-butyl-D-[c(RGDfK)]-[c(RGDy(I)K)] (10)

The iodination of compound **5** was prepared according to literature [58]. The solution of compound **5** (10 mg, 7.00 μmol) in water (0.5 mL) was treated *N*-iodosuccinimide (0.3 mg, 1.40 μmol) in CH_3CH (0.5 mL). The mixture was stirred at room temperature for 15 min. The solution was diluted with water and followed by a semi-preparative HPLC purification. The expected product ((N_3-butyl-D-[c(RGDfK)]-[c(RGDyK)]) was collected at 22.8 min. After the resulting solution was dried under reduced pressure, it gave compound **10** (1.2 mg, 12%) as white solid: MS (ESI) *m/z* 1557.4 $(M + H)^+$, 779.5 $(M + 2H)^{2+}$

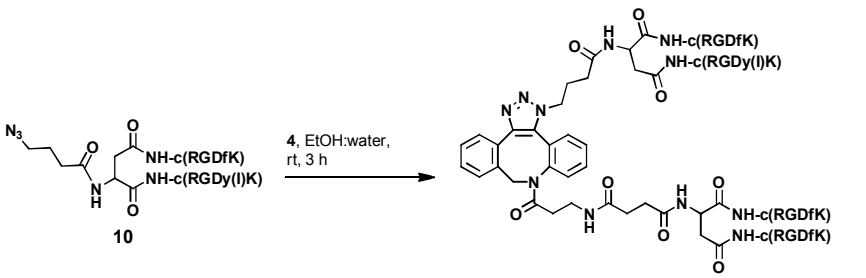

11 (ADIBOT-D_2-[c(RGDy(I)K)]-[c(RGDfK)]$_3$, 52%)

ADIBOT-D_2-c(RGDy(I)K)-[c(RGDfK)]$_3$ (11)

ADIBOT = aza-dibenzocycloocta-triazoles

The solution of compound **7** (2 mg, 1.20 μmol) in 0.5 mL of solvent mixture with EtOH and water (v/v = 1/1) was treated compound **3** (1.7 mg, 1.20 μmol) in 0.5 mL of solvent mixture with EtOH and water (v/v = 1/1). The mixture was stirred at room temperature for 3 h . The solution was diluted with water and followed by the HPLC purification. The product was collected at 22.1 min. After the resulting solution was dried under reduced pressure, it gave ADIBOT-D_2-[c(RGDy(I)K)]-[c(RGDfK)]$_3$ (**11,** 2 mg, 52%) as white solid: MS (ESI) *m/z* 1610.5 $(M + 2H)^{2+}$, 1073.7 $(M + 3H)^{3+}$ 805.5 $(M + 4H)^{4+}$

3. Fluorescent dyes conjugation with RGD peptides

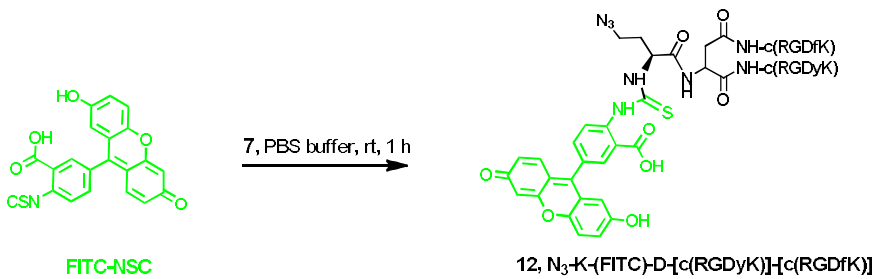

N_3-K-FITC-D-[c(RGDyK)]-[c(RGDfK)] (12)

The compound **7** (5 mg, 2 μmol) was dissolved in PBS buffer (0.5 mL, pH 7.5) in a vial and added FITC-NCS (2 mg, 4 μmol). The mixture was stirred at room temperature for 1 h. The solution was diluted with water and separated by gel filteration column. After the resulting solution was dried under reduced pressure, it gave N_3-K-FITC-D-[c(RGDyK)]-[c(RGDfK)] (**12,** 3 mg, 72%) as yellow solid: MS (ESI) *m/z* 1862.6 $(M + H)^+$, 932.5 $(M + 2H)^{2+}$.

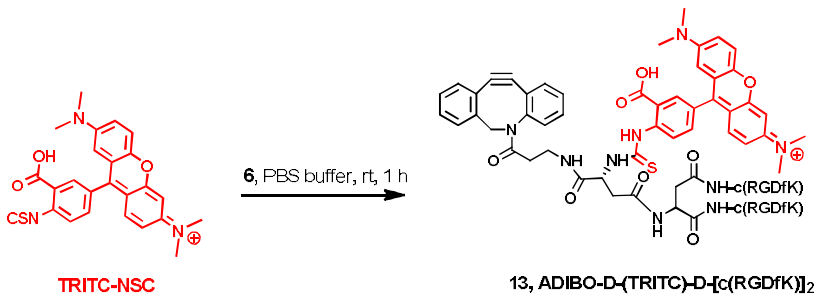

ADIBO-D-TRITC-D-[c(RGDfK)]$_2$ (13)

The compound **6** (5 mg, 2 μmol) was dissolved in PBS buffer (0.5 mL, pH 7.5) in vial and added TRITC-NCS (2 mg, 4 μmol).

The mixture was stirred at room temperature for 1 h. The solution was diluted with water and separated by gel filteration column. After the resulting solution was dried under reduced pressure, it gave ADIBO-D-(TRITC)-D-[c(RGDfK)]$_2$ (**13**, 3.1 mg, 75%) as pink solid: MS (ESI) *m/z* 2122.9 $(M + H)^+$, 1061.9 $(M + 2H)^{2+}$, 708.5 $(M + 3H)^{3+}$

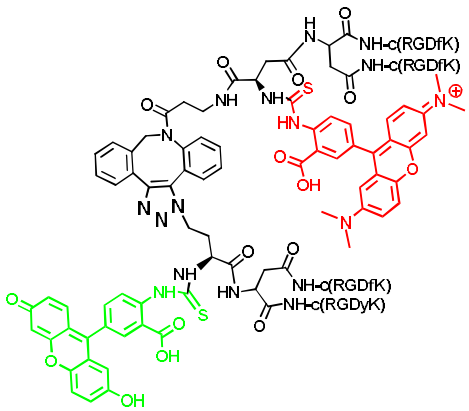

ADIBOT-K-D-FITC-TRITC-D$_2$-c(RGDyK)-[c(RGDfK)]$_3$ (14)

ADIBOT = aza-dibenzocycloocta-triazoles

The solution of compound **12** (2 mg, 1.00 μmol) in 0.5 mL of solvent mixture with EtOH and water (v/v = 1/1) was treated compound **13** (2.1 mg, 1.00 μmol) in 0.5 mL of solvent mixture with EtOH and water (v/v = 1/1). The mixture was stirred at room temperature for 3 h. The solution was diluted with water and separated by gel filteration column. After the resulting solution was dried under reduced pressure, it gave **14** (2.8 mg, 76%) as pink solid: MS (ESI) *m/z* 1993.7 $(M + 2H)^{2+}$, 1329.4 $(M + 3H)^{3+}$ 997.3 (M +

4H)$^{4+}$

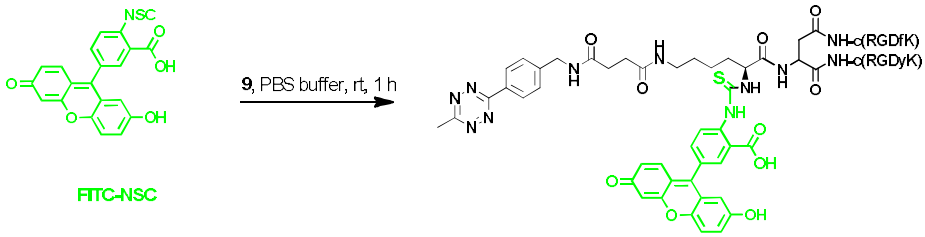

Tz-K-FITC-D-[c(RGDyK)]-[c(RGDfK)] (15)

The compound **9** (5 mg, 3 μmol) was dissolved in PBS buffer (0.5 mL) in a vial and added FITC-NCS (2.6 mg, 6 μmol). The mixture was stirred at room temperature for 1 h. The solution was diluted with water and separated by gel filteration column. After the resulting solution was dried under reduced pressure, it gave Tz-K-FITC-D-[c(RGDyK)]-[c(RGDfK)] (**15,** 3 mg, 72%) as yellow solid: MS (ESI) *m/z* 2120.8 $(M + H)^{+}$, 1060.9 $(M + 2H)^{2+}$.

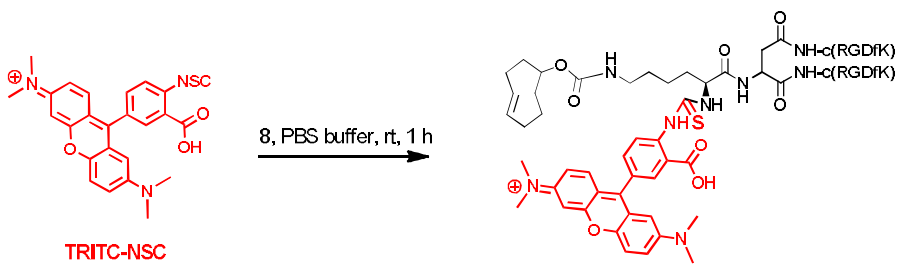

TCO-K-TRITC-D-[c(RGDfK)]$_2$ (16)

The compound **8** (5 mg, 3 μmol) was dissolved in PBS buffer (0.5 mL) in vial and added TRITC-NCS (2.6 mg, 6 μmol). The mixture was stirred at room temperature for 1 h. The solution was diluted with water and separated by gel filteration column. After the resulting solution was dried under reduced pressure, it gave **16** (4.8 mg, 80%) as pink solid: MS (ESI) *m/z* 2028.9 $(M + H)^+$, 1014.5 $(M + 2H)^{2+}$, 676.6 $(M + 3H)^{3+}$

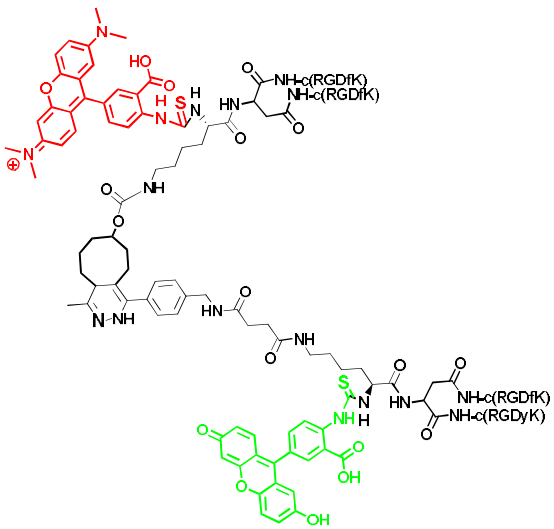

Dihydropyrazine-K$_2$-FITC-TRITC-D$_2$-c(RGDyK)-[c(RGDfK)]$_3$ (17)

The solution of compound **15** (2 mg, 1.00 μmol) in 0.5 mL of solvent mixture with EtOH and water (v/v = 1/1) was treated compound **16** (2 mg, 1.00 μmol) in 0.5 mL of solvent mixture with EtOH and water (v/v = 1/1). The mixture was stirred at room temperature for 3 h. The solution was diluted with water and

separated by gel filteration column. After the resulting solution was dried under reduced pressure, it gave **17** (2.8 mg, 69%) as pink solid: MS (ESI) *m/z* 2075.8 $(M + 2H)^{2+}$, 1384.2 $(M + 3H)^{3+}$ 1038.4 $(M + 4H)^{4+}$

4. Radioiodo-labeling of RGD peptides

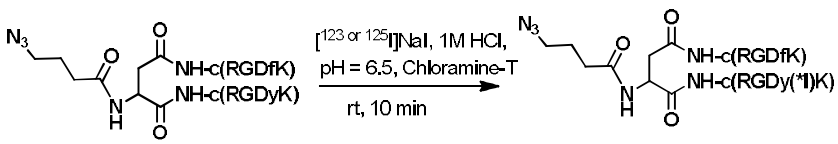

5 **[^{123} or ^{125}I]10**

N_3-butyl-D-[c(RGDfK)]-[c(RGDy(^{123}I)K)] ([^{123}I]10)

To [^{123}I]NaI solution (740 MBq) in 1 M NaOH, 1 M HCl (50 μL) was added to adjust pH 6.5. The solution of precursor (**5**) (0.2 mg) in water (100 μL) and chloramine-T in water (100 μL) was added to [^{123}I]NaI solution. The reaction mixture was stirred at room temperature for 10 min. The crude mixture was diluted with excess water and passed through into plus tC18 Sep-Pak then eluted with 90% methanol-water (2 mL). The resulting solution was purified with semi-preparative HPLC system. The expected product [^{123}I]**10** was collected at 21.5 min and radiochemical yield was 34.0 ± 6.5%, decay-corrected. The obtained solution was loaded into plus tC18 Sep-Pak and exchanged to 10% ethanol-water.

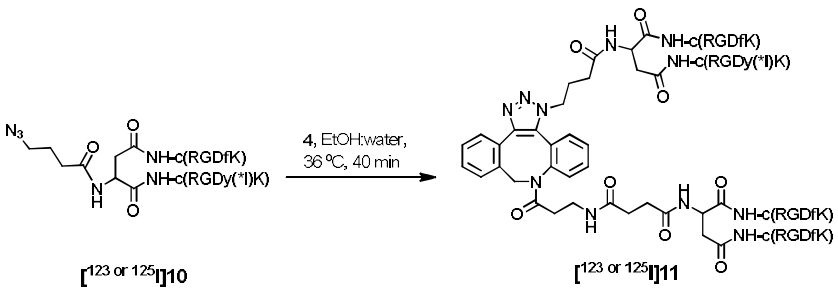

[^{123} or ^{125}I]**10** [^{123} or ^{125}I]**11**

ADIBOT-D$_2$-[c(RGDy(^{123}I)K)]-[c(RGDfK)]$_3$ ([^{123}I]11)

The solution of [^{123}I]**10** (185 MBq) in water (200 μL) was treated to ADIBO-D-[c(RGDfK)]$_2$ (**4**) in ethanol (200 μL). This mixture was stirred with bubbling nitrogen at 36 ^{o}C for 40 min. The crude mixture was diluted with water and purified with semi-preparative HPLC system. The expected product [^{123}I]**11** was collected at 17.5 min and radiochemical yield was 59.3 ± 4.0%, decay-corrected. The resulting solution was loaded into plus tC18 Sep-Pak and exchanged to 10% ethanol-water.

5. In vitro evaluation of RGD peptides

Human serum stability

The stability of **[^{123}I]10** and **[^{123}I]11** was analyzed by monitoring the Radio-TLC. Human whole blood was centrifuged at 3500 rpm for 5 min, and the supernatant was collected into new tube. An aliquot (3.7 MBq) of ^{123}I-N_3-RGD dimer and ^{123}I-Tz-RGD tetramer in 10% ethanol-saline (0.1 mL) was added to human serum (0.5 mL) and the mixture incubated at 37 ^{o}C for 4 h. At each time point (10, 30, 60, 120, and 240 min), the sample (0.1 mL) was taken and added to acetonitrile (0.1 mL). After vortexing (30 s), the mixture was centrifuged at 3,500 rpm for 5 min. The obtained supernatant was analyzed by radio-TLC using 100% acetone as the developing solvents. R_f value was 0 for ^{123}I-N_3-RGD dimer and ^{123}I-Tz-RGD tetramer and 0.9 for free iodine, respectively.

Flow cytometric assay

Cells were detached with 0.05 M trypsin/EDTA solution and washed with cold PBS (10 mM) twice. Cells were prepared in FACS tube (BD bioscience) at a concentration of 5 x 10^5 cells/ 100 μL of 10 mM PBS containing 1% bovine serum albumin (BSA, Sigma-Aldrich). The cells were incubated with anti-integrin alpha V beta 3 (Abcam, FITC-conjugated) or the isotype control antibody (mouse IgG1 kappa [MOPC-21] FITC, Abcam) for 1 h at 4℃ with constant shaking using thermomixer (Eppendorf). After incubation, the stained cells were washed twice with cold PBS containing 1% BSA and analyzed using Guava® easy Flow Cytometer and InCyte™ GuavaSuite Software (Merck).

Binding assay

The receptor binding affinity studies of **[^{123}I]10** and **[^{123}I]11** were performed using ^{125}I-c(RGDyV) as the integrin-specific radio-ligand [36]. The 100 μL of a cell suspension in microcentrifuge tubes were incubated with ^{125}I-c(RGDyV) (0.037 MBq/tube) in the presence of increasing concentrations of I-N_3-RGD dimer and I-Tz-RGD tetramer. The tubes were centrifuged at 2,000 rpm at 4 ^{o}C, respectively. Centrifuged cell pellets were washed three times with cold PBS (1 mL). The radioactivity was determined using a gamma counter (Wizard 1480, wallac).

FRET microscopy

U87-MG cells were plated on glass bottom confocal dish (SPL Life Science) round cover glasses (seeding density of 1 × 10^6 cells/3 mL of complete DMEM). Cells were grown for 48 h at 37℃ with 5 % CO_2 atmosphere. The medium discarded and the cells were rinsed with 2 mL of PBS buffer for twice. Cells were treated with both of **12** (50 μM) and **13** dimer (50 μM) or only **14** (50 μM) or blocking and incubated for 2 h at 37 ^oC. After incubation, cells were washed three times with 2 mL of cold PBS. 4% paraformaldehyde was added in each dish for fixation. Fixation was performed for 1 h at room temperature in the dark condition. The confocal imaging and FRET measurements were carried out on an inverted confocal microscope (Nikon A1 Rsi). Two different band path filters, namely, 490/525, and 557/576 nm, to collect the emission signal from FITC and FRET, respectively, upon irradiation with the same excitation laser (490 nm for FITC excitation, 576 nm for TRITC emission).

6. Ex/In vivo evaluation of RGD Peptides

Ex vivo biodistribution

Ex vivo biodistribution studies were performed in U87-MG tumor bearing mouse model. The mice were injected with **[^{123}I]10** and **[^{123}I]11** and using sequential targeting (0.74 MBq, 200 μL in saline) into the tail vein, sacrificed at the indicated time points (n = 4, 10, 30, 60 and 120 min). Blood, tumor, and normal organs (heart, liver, lung, spleen, kidneys, small intestine, large intestine, muscle, thyroid, brain and femur) were extracted and measured for radioactivity using a gamma counter. Data was presented as the percentage of the injected dose per gram of tissue in comparison with samples of a standard dilution of the initial dose (%ID/g).

Small Animal SPECT/CT Imaging

High-resolution SPECT scans of each mouse for 90 or 120 min after the intravenous injection of radiotracers (18.5 MBq, n = 3). Mice were placed in a prone position on the bed under anesthesia with 2% isoflurane. Whole body mouse SPECT/CT imaging perforemd on a Nano SPECT/CT tomograph (Bioscan) equipped with 4 NaI detectors and fitted with 1.4 mm mouse wholebody multi-pinhole collimator with 9 pinholes (full width at half maximum ≤ 1.2 mm). A total of 14 projections were acquired in a 256 × 256 acquisition matrix with a 15 s per projection. Images were reconstructed using a

2D ordered-subset expectation maximization algorithm (9 iteration). Cone-beam CT images were acquired (180 projection, 500 ms/projectoin, 45 kVp) before SPECT imaging. Co-registration of SPECT and CT images was performed using InvivoScope software (Bioscan). The SPECT imaging was followed by CT image acquisition with the animal in exactly the same position.

RESULTS

1. Preparation of RGD peptides

The dimeric RGD peptides (NH_2-D-[c(RGDfK)]$_2$ (**1**) and NH_2-D-[c(RGDyK)]-[c(RGDfK)] (**3**)) were designed as ligands for integrin $\alpha_v\beta_3$, based on the previous studies [44]. The functional groups for azide/ADIBO and tetrazine/TCO click reaction were incorporated into the peptides as shown in the schemes below (**Figure 8, 9**). The **3** was designed to contain a cyclic RGDyK for radiolabeling, which includes a tyrosine residue to label with ^{123}I or ^{131}I.

NH_2-D-[c(RGDfK)]$_2$ (**1**) was synthesized by amide condensation of *N*-(*tert*-butoxycarbonyl)-L-aspartic acid and the protected c(RGDfK)-NH_2 peptide followed by deprotection of Pbf and *tert*-butyl groups. NH_2-D-[c(RGDyK)]-[c(RGDfK)] (**3**) was obtained from amide coupling of *N*-(*tert*-butoxycarbonyl)-L-aspartic acid 4-benzyl ester and c(RGDyK)-NH_2 followed by the deprotection of the benzyl group in the presence of 10% palladium on charcoal under hydrogen atmosphere to get the intermediate (**2**). To make RGD dimer, amino group of c(RGDfK)-NH_2 was linked with Boc-NH-D-[c(RGDyK)]-COOH (**2**), followed by the deprotection of Boc group.

The compounds **4**, **6**, and **8** was prepared by amide coupling

between **1** and ADIBO or TCO moiety and the compounds **5**, **7**, and **9** was synthesized by amide condensation of azide or tetrazine moiety and **3**. Especially, **6**, **7**, **8**, and **9** included $-NH_2$ group for conjugation with fluorescent dyes. All RGD peptides were purified by HPLC system with >98% purity and confirmed by LC-MS.

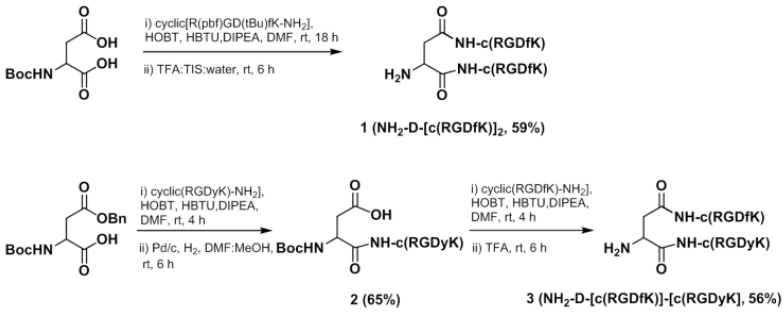

Figure 8. Synthesis of cyclic RGD peptides.

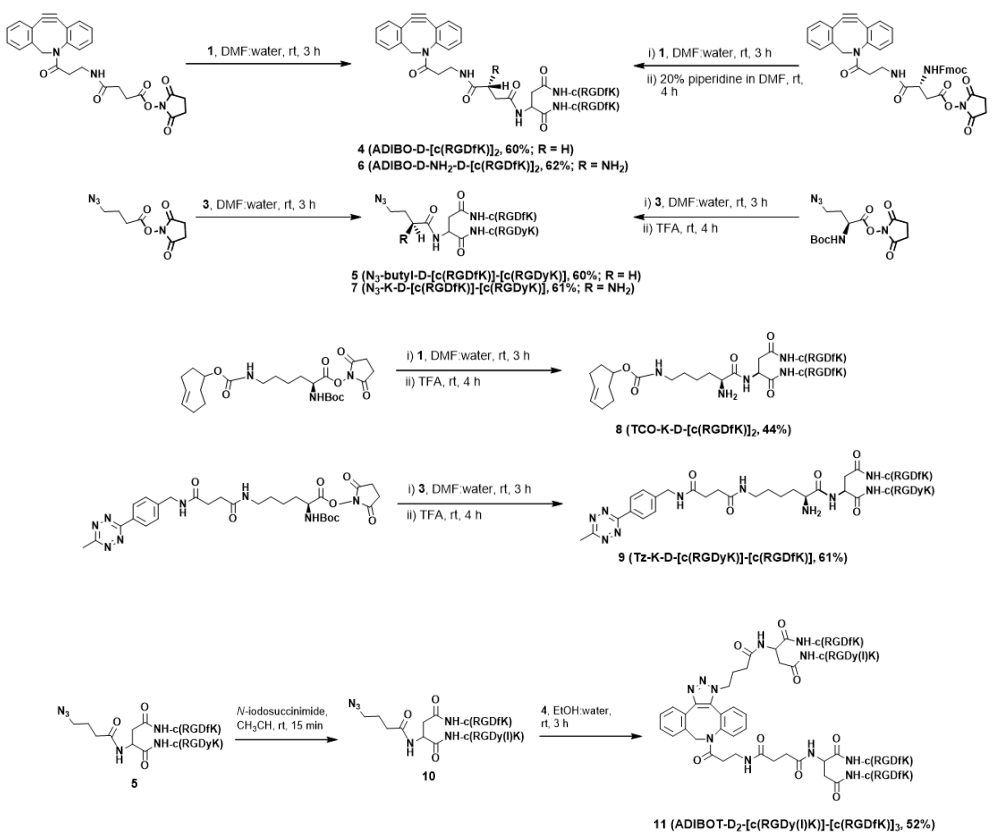

Figure 9. Synthesis of cyclic RGD peptides for click reaction

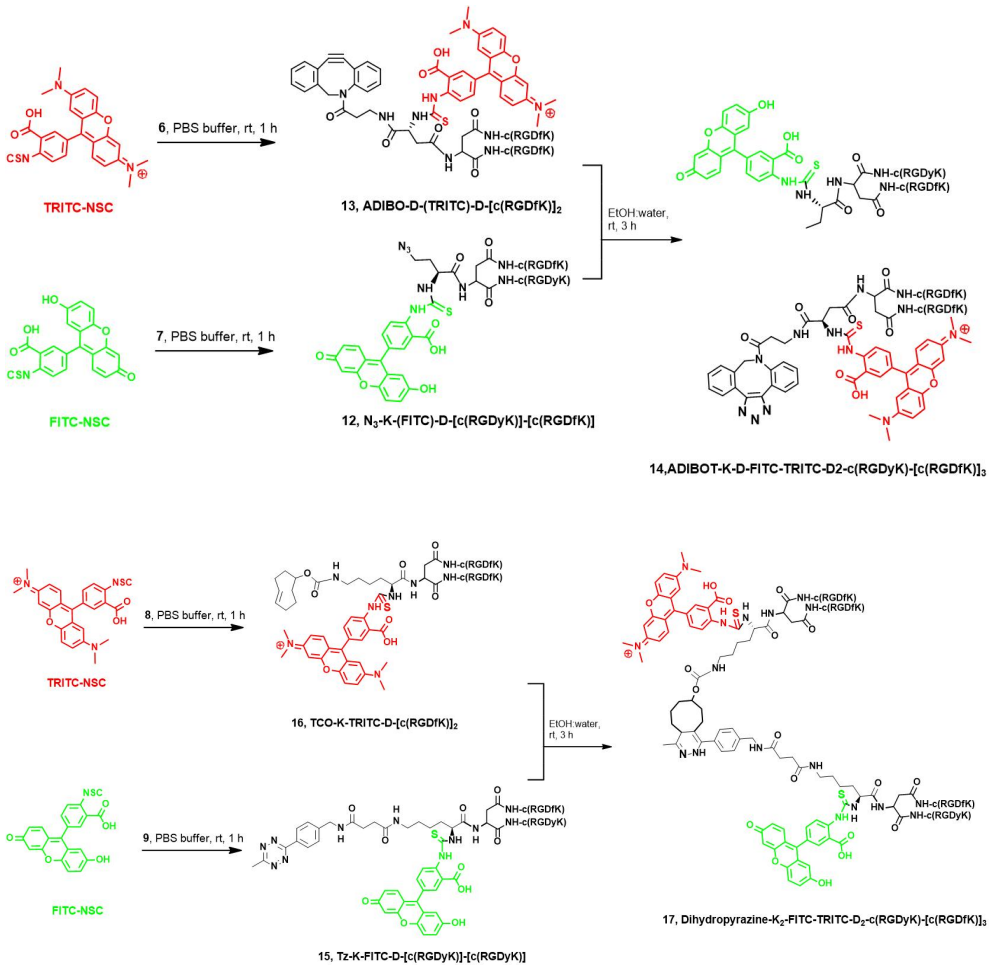

Figure 10. Synthesis of fluorescent conjugated cyclic RGD peptides

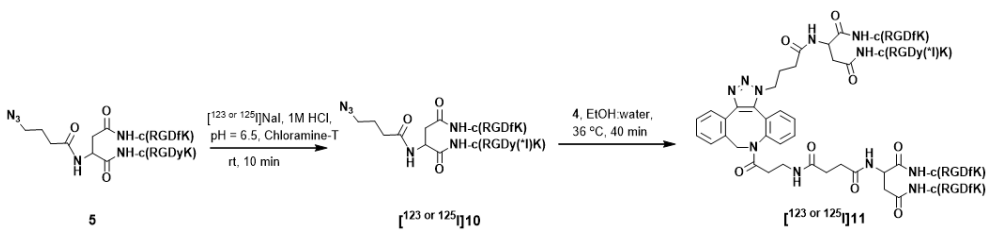

Figure 11. Radiolabeling of cyclic RGD peptides

2. Fluorescent dyes conjugated RGD peptides

For the confocal imaging, two fluorescence dyes, FITC (fluorescein-isothiocyanate) and TRITC (tetramethylrhodamine) were conjugated to the peptides for in vitro FRET assays. After preparing NH_2-D-[c(RGDfK)]$_2$ (**1**) and NH_2-D-[c(RGDyK)]-[c(RGDfK)] (**3**), aspartic acid or lysine residue of each RGD peptide was conjugated with a fluorescence dye (**Figure 10**).

Then, FITC or TRITC conjugated RGD peptides (**12-17**) were synthesized by amide condensation of amine moiety of RGD peptides and isocyanate moiety of dyes. The fluorescent dye labeled RGD dimers were purified by size exclusion chromatography.

3. Radioiodo-labeled RGD peptides

The N_3-butyl-D-[c(RGDfK)]-[c(RGDy(I)K)] (**10**) as the cold standard were prepared according to reference [54]. In the presence of **5**, *N*-iodosucciniimide (1.2 equiv.) in CH_3CH (0.5 mL) was treated and the mixture was stirred at room temperature for 15 min. ADIBOT-D_2-c(RGDy(I)K)-[c(RGDfK)]$_3$ **(11)** was synthesized via click reaction between prepared **10** and **4**. After the reaction, both **10** and **11** were purified with a semi-preparative HPLC system.

For the radiolabeling of **5**, the precursor was mixed with [^{123}I]NaI (740 MBq) and chloramine T (3.3 equiv.) as an oxidant (**Figure 11**).

The mixture was incubated at room temperature for 10 min. After incubation, the reaction mixture was purified by a semi-preparative HPLC system and the desired product (**[^{123}I]10**) was obtained at 18.7 min with 34.0 ± 6.5% radiochemical yields (*n* = 4, decay-corrected) and high purity (> 99%). The identity of the compound was confirmed by co-injection with a cold compound (**Figure 12**).

To compare tumor uptake of new strategy, **[^{123}I]11** was prepared by using conjugation of **[^{123}I]10** and **4** (**Figure 10**). The reaction was carried out in ethanol/water (v/v = 1/1) at 36℃ for 1 h. The reaction mixture was purified by a semi-preparative HPLC system. The product (**[^{123}I]11**) was obtained at 15.4 min with adequate radiochemical yield (59.3 ± 4.0%, *n* = 3, decay-corrected) and high purity (>99%). The identity of the compound was confirmed by co-injection with a cold compound (**Figure 13**).

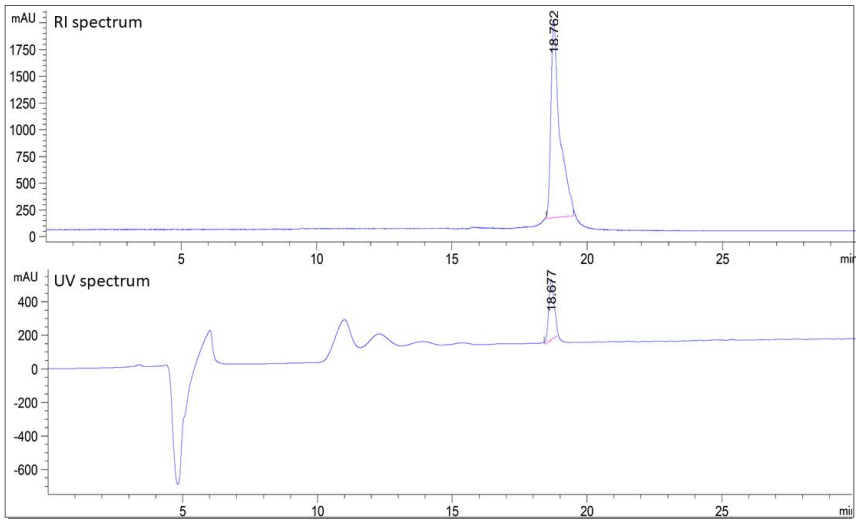

Figure 12. HPLC profile for co-injection with **[^{123}I]10** and **10**

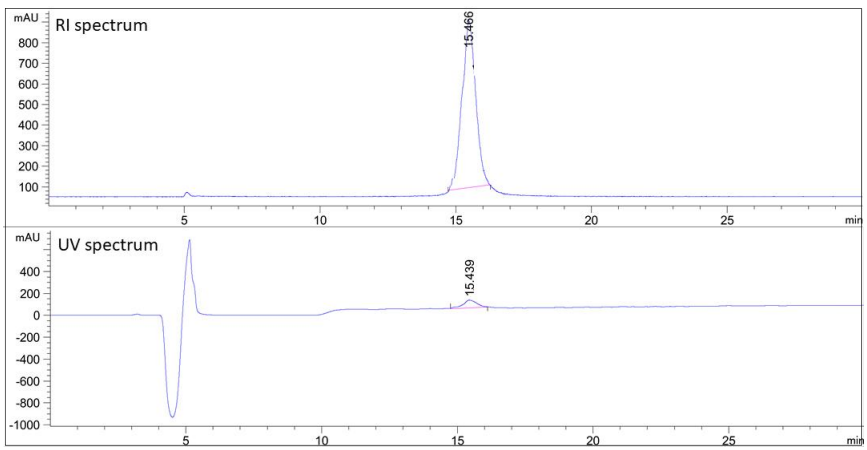

Figure 13. HPLC profile for co-injection with **[^{123}I]11** and **11**.

4. In vitro experimental results

In vitro intermolecular conjugation

Before in vitro and in vivo analysis using U87-MG cells, reaction time of the click reaction was evaluated by using HPLC system. Moreover, reaction rate between azide-ADIBO pair and tetrazine-TCO pair was assessed to investigate the efficiency of the click moiety.

A solution of N_3-K-FITC-D-[c(RGDyK)]-[c(RGDfK)] (**12**) or Tz-K-FITC-D-[c(RGDyK)]-[c(RGDfK)] (**15**) in distilled water/PBS buffer (v/v =1/1) was treated with ADIBO-D-TRITC-D-$[c(RGDfK)]_2$ (**13**) or TCO-K-TRITC-NH_2-D-$[c(RGDfK)]_2$ (**16**) for 40 min at room temperature. Aliquot of the reaction mixture was analyzed using an HPLC system at 0, 10, 20, 30, and 40 min (**Figure 14**). The results showed that the reaction time was shorter for tetrazine-TCO pair by approximately 10 min.

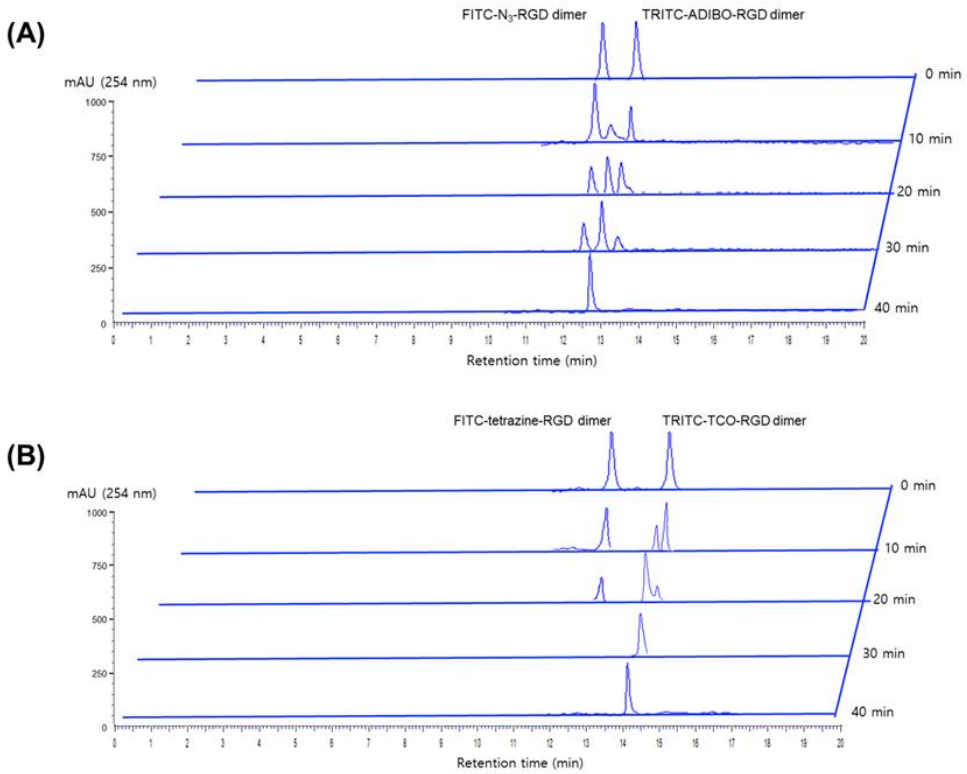

Figure 14. Comparison with time of click reaction. (A) HPLC chromatograms during the click reaction with aizide and ADIBO moiety at 0, 10, 20, 30, and 40 min. Identification of **12** (T_R = 12.0 min), **14** (T_R = 12.7 min), **13** (T_R = 13.5 min). (B) HPLC chromatograms during the click reaction with tetrazine and TCO moiety at 0, 10, 20, 30, and 40 min. Identification of **15** (T_R = 13.0 min), **17** (T_R = 14.0 min), **16** (T_R = 14.7 min).

Human serum stability

The stability of **[^{123}I]10** and **[^{123}I]11** was determined by radio thin layer chromatography using acetone as a developing solvent. **[^{123}I]10** and **[^{123}I]11** were sufficiently stable in human serum at 36 ^{o}C for 4 hours and only 4 % of **[^{123}I]10** and 7 % of **[^{123}I]11** were dissociated. These results indicate that radiolabeled RGD peptides would evaluate in vivo the expression level of integrin $\alpha_v\beta_3$ on tumor and in vivo intermolecular click reaction without degradation.

Integrin $\alpha_V\beta_3$ expression on U87-MG cells

Before performing the in vitro and in vivo analysis, the expression of integrin $\alpha_V\beta_3$ on U87-MGU87-MG cells was determined by flow cytometric assay. While integrin $\alpha_V\beta_3$ positively expressed on U87-MGU87-MG cells, it was not found on the negative control A549 cells (**Figure 15**). Thus, U87-MG cells were sufficiently suitable for in vitro and vivo experiments.

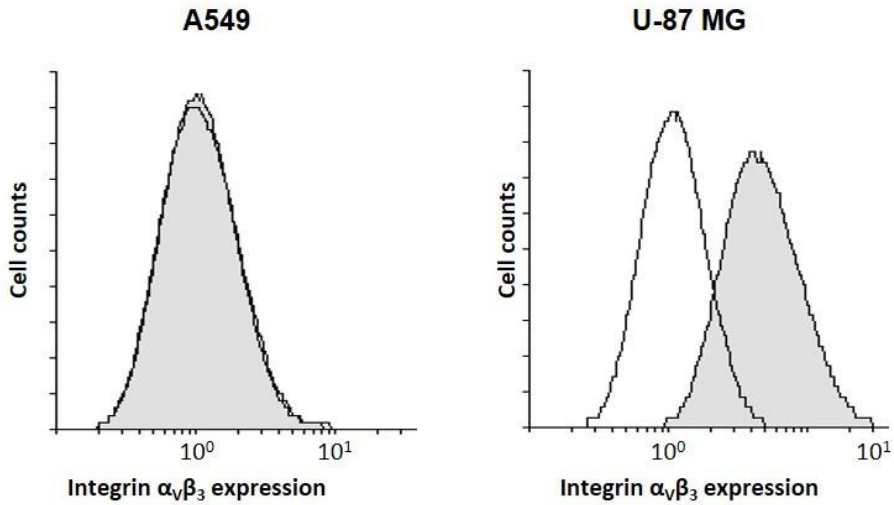

Figure 15. Flow cytomtric analysis for integrin $\alpha_V\beta_3$ expression of A549 and U87-MG cell lines. Cells were incubated with isotype control antibody (black line histogram) or anti-integrin $\alpha_V\beta_3$ (gray filled histogram). Isotype antibody was used as a control. The mean of fluorescence intensities were 12.69 (A549) and 55.50 (U87-MG), respectively.

In vitro binding affinity for integrin $\alpha_V\beta_3$

The binding affinity of N_3-butyl-D-[c(RGDfK)]-[c(RGDy(I)K)] **(10)** and ADIBOT-D_2-c(RGDy(I)K)-[c(RGDfK)]$_3$ **(11)** for integrin $\alpha_v\beta_3$ was determined in a competitive cell binding assay. Binding of **10** and **11** to integrin $\alpha_v\beta_3$ was competed by ^{125}I-c(RGDyV) in a concentration-dependent manner on U87-MG cells. The IC_{50} values of **10** and **11** were 1.08 ± 0.08 nM and 0.52 ± 0.12 nM, respectively (**Table 2**). The binding affinity for integrin $\alpha_v\beta_3$ on U87-MG cells of **11** (tetramer form) was slightly higher than that of **10** (dimer form).

Table 2. Affinities (IC_{50}, nM) for integrin $\alpha_v\beta_3$[a]

Compound	IC_{50} (nM)
10	1.08 ± 0.08
11	0.52 ± 0.12

[a]The in vitro binding affinity (Ki, nM) was measured by competition with ^{125}I-c(RGDyV) on U87-MG cells.

In vitro blocking study

The blocking study, which can confirm the selectivity, performed on U87-MG cells by using confocal imaging (**Figure 16**). FITC conjugated RGD peptides (N_3-K-FITC-D-[c(RGDyK)]-[c(RGDfK)] **(12)**, and c(RGDyK) as blocker were prepared for in vitro cell assays. In the results, fluorescent signals of FITC were observed on cancer cell in treatment of **12** but, **12** blocking with c(RGDyK) not showed fluorescent signals. This results indicated that ligand for this study selectively bound to integrin $\alpha_v\beta_3$.

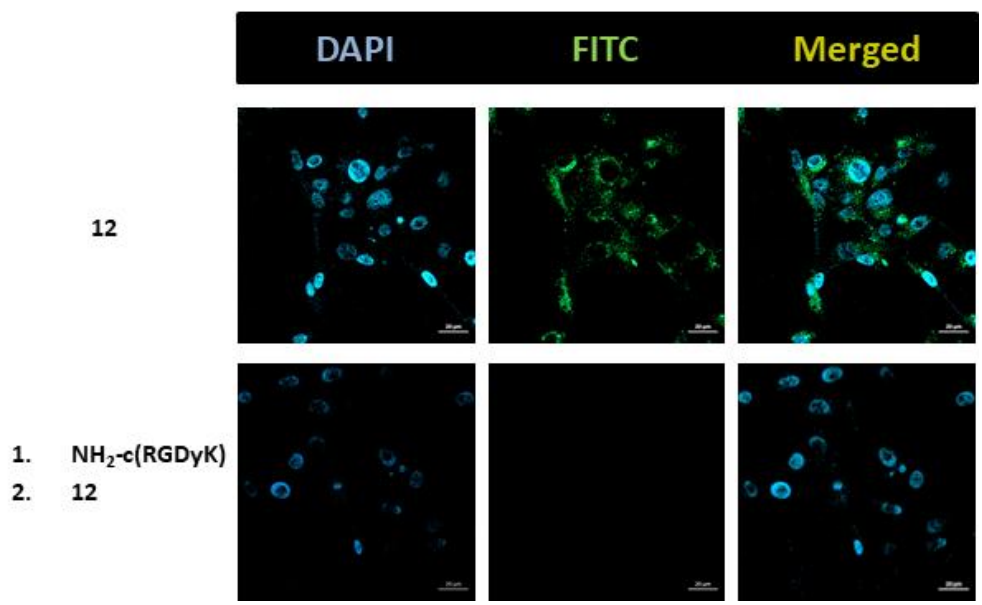

Figure 16. In vitro blocking study with c(RGDyK) on U87-MG cells. Condition; N_3-K-FITC-D-[c(RGDyK)]-[c(RGDfK)] (**12**), **12** blocking with c(RGDyK)

In vitro confocal microscopy imaging on U87-MG cells

FRET imaging, which can be an accurate measurement of molecular proximity at nanometer distances (1-10 nm), allows the detection of intermolecular conjugation. To identify intermolecular conjugation of RGD peptides on U87-MG cells, FITC or TRITC conjugated RGD peptides (N_3-K-FITC-D-[c(RGDyK)]-[c(RGDfK)] **(12)**, ADIBO-D-TRITC-D-$[c(RGDfK)]_2$ **(13)** and ADIBOT-K-D-FITC-TRITC-D_2-c(RGDyK)-$[c(RGDfK)]_3$ **(14)**) were prepared for in vitro FRET analysis. For the in vitro assay, three groups was considered: control, blocking and treatment group. The control group was treated with one of fluorescent conjugated RGD peptide (**12** or **13**). The pre-conjugated RGD peptide between **12** and ADIBO-NH_2 (3-amino-1-(11,12-didehydrodibenz[*b,f*]azocin-5(6*H*)-yl)-1-propanone) was treated as a dummy for blocking intermolecular conjugation, which could help identify FRET signals that indicate whether or not an intermolecular interaction between RGD peptides has occurred. The treatment group included two conditions for comparing effect of intermolecular conjugation. One was treated **14** and the other was sequentially treated **12** and **13**. The results are shown in **Figure 17, 18**.

In the control group, fluorescent signals of **12** or **13** in each FITC and TRITC channel located in the cells (**Figure 17**). In blocking group, each fluorescent signals of FITC and TRITC were observed on cells but there were no FRET signals. This suggest that FRET signals

can show intermolecular click reaction. In condition of sequentially treating **12** and **13**, each fluorescent signals of FITC and TRITC were located inside the cells and they were co-localized. Moreover, the high intensity of FRET signals were observed in the merged site of FITC and TRITC inside of tumor cells (**Figure 18**). In contrast, although FITC and TRITC signals of **14** were observed inside the cells, the FRET signals shown low intensity. These results indicated that strategy of this study can induce internalization of RGD peptides via intermolecular conjugation, which occurred from FITC on **12** to TRITC on **13**, and enhancement of tumor uptake.

Futhermore, RGD peptides conjugated with TCO and tetrazine for click reaction were analyzed by confocal microscopy imaging on U87-MG cells in following the above conditions, which were control, blocking and treatment group. The control group was treated with one of fluorescent conjugated RGD peptide (**15** or **16**). The pre-conjugated RGD peptide between **15** and ADIBO-NH_2 (3-amino-1-(11,12-didehydrodibenz[*b,f*]azocin-5(6*H*)-yl)-1-propanone) was treated as a blocking group. The treatment group included two conditions that were treated only **17** or sequentially addition of **15** and **16**. The results are shown in **Figure 19, 20**.

The results were similar with assay of RGD peptides, which conjugated with ADIBO and azide moiety. In the control group, fluorescent signals of **15** or **16** in each FITC and TRITC channel located in the cells (**Figure 19**). In blocking group, each fluorescent signals of FITC and TRITC were observed on cells but there were no

FRET signals. In condition of sequentially treating **15** and **16**, each fluorescent signals of FITC and TRITC were located inside the cells and they were co-localized. Moreover, the higher FRET signals than treatment of **17** were observed in the merged site of FITC and TRITC inside of tumor cells (**Figure 20**).

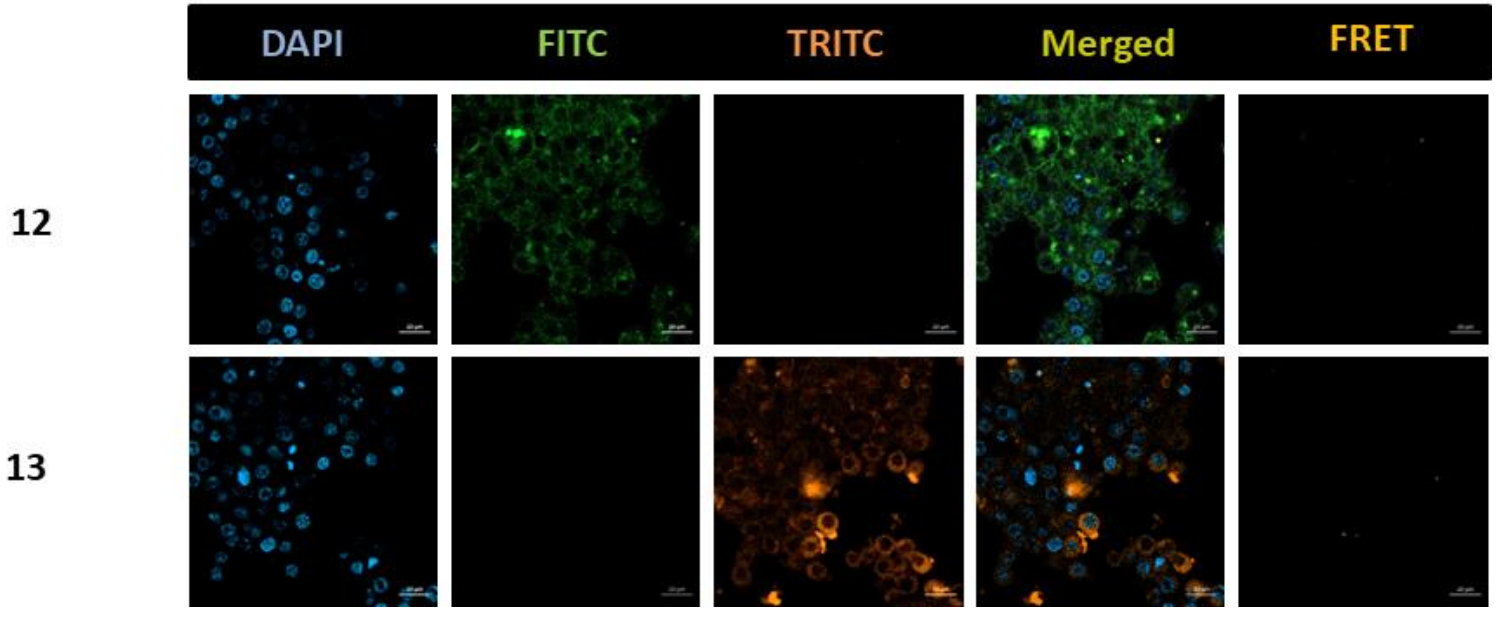

Figure 17. Images of confocal microscopy in control group on U87-MG cells. Condition; N_3-K-FITC-D-[c(RGDyK)]-[c(RGDfK)] (**12**), ADIBO-D-TRITC-D-[c(RGDfK)]$_2$ (**13**).

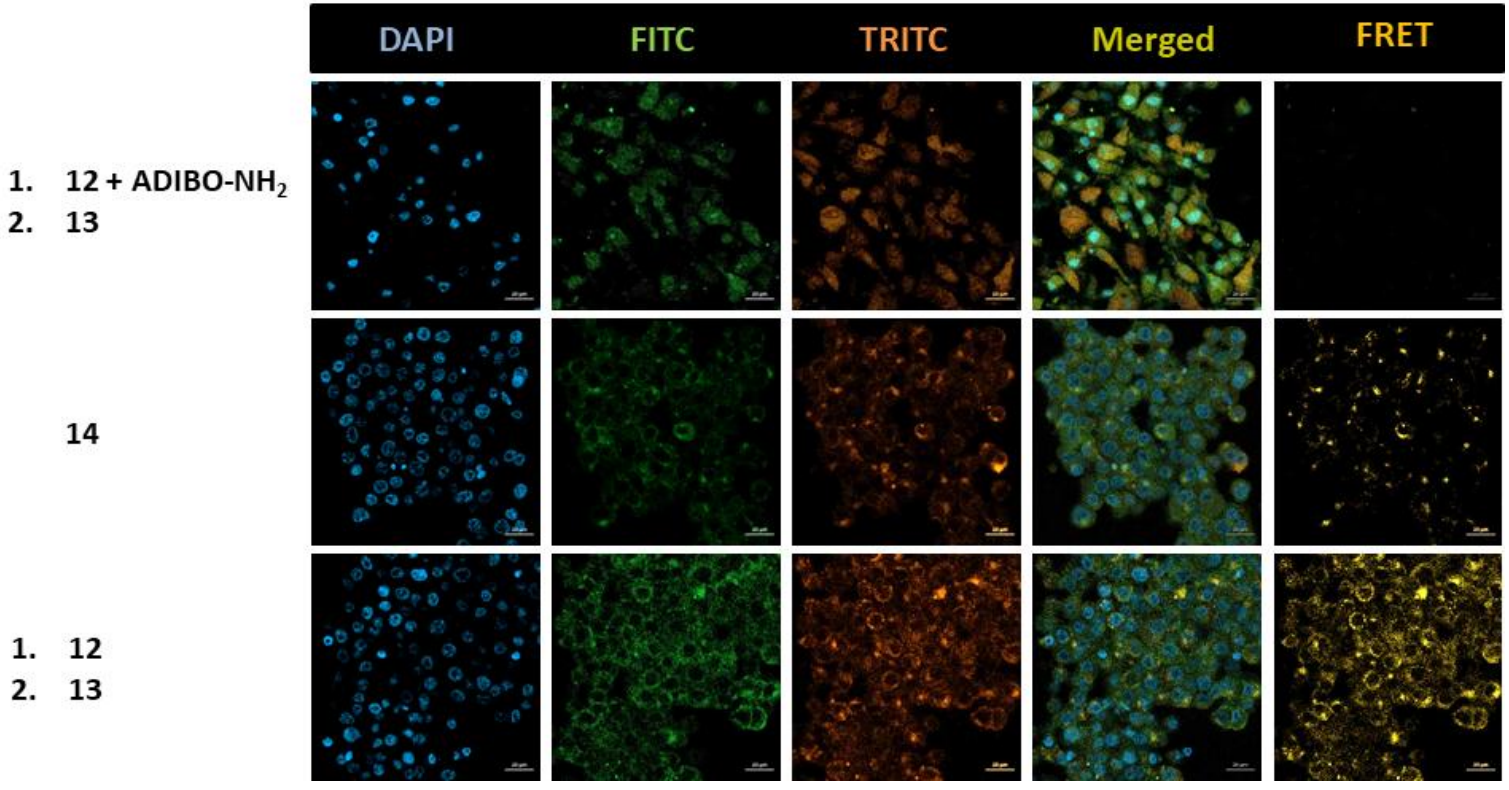

Figure 18. Images of FRET microscopy in U87-MG cells. Condition; **12** blocking with ADIOBO-NH_2 and **13**, only **14**, sequentially treatment of **12** and **13**.

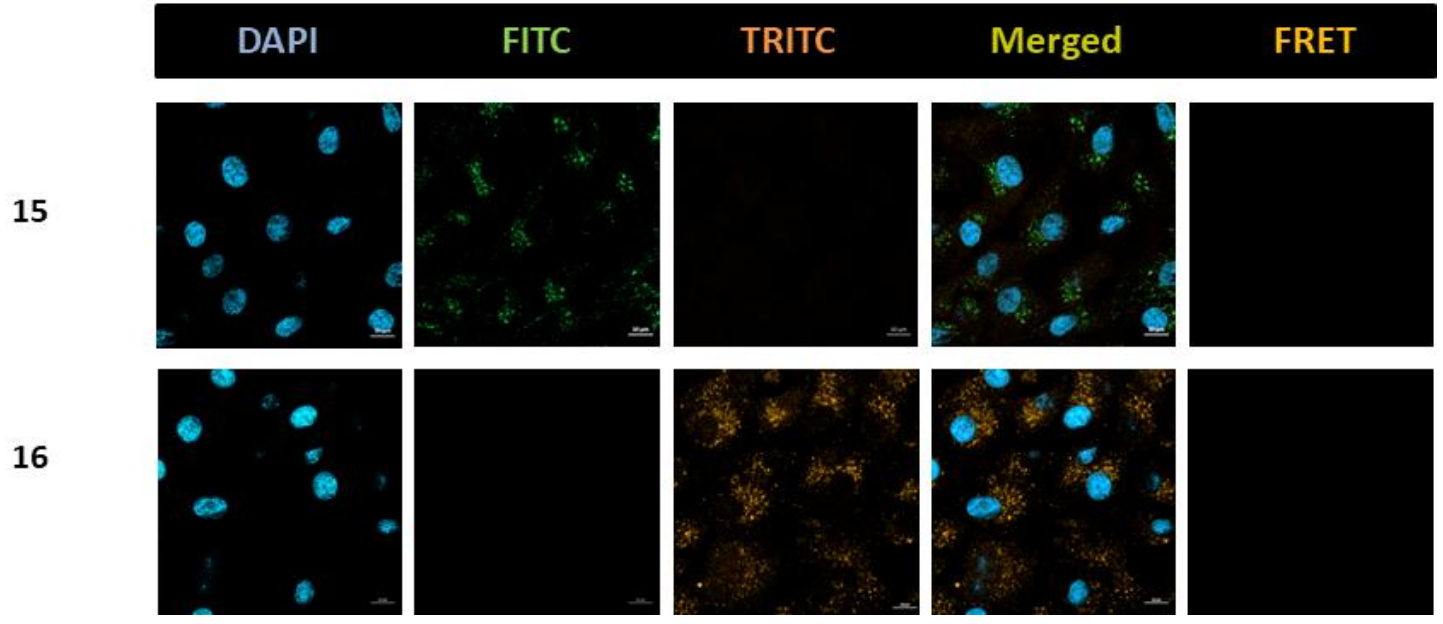

Figure 19. Images of confocal microscopy in control group on U87-MG cells. Condition; Tz-K-FITC-D-[c(RGDyK)]-[c(RGDfK)] (**15**), TCO-K-TRITC-D-[c(RGDfK)]$_2$ (**16**).

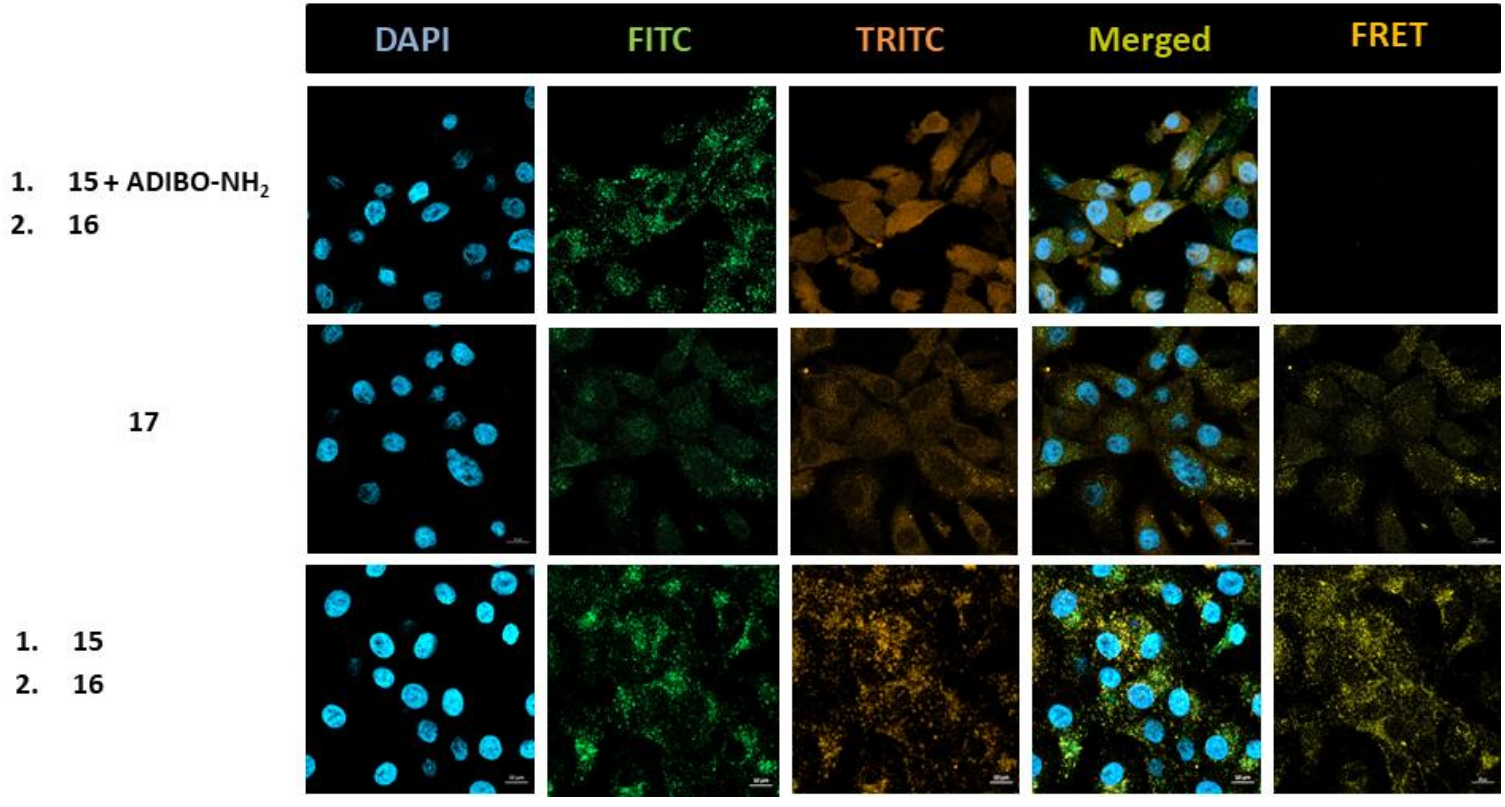

Figure 20. Images of FRET microscopy in U87-MG cells. Condition; **15** blocking with ADIOBO-NH_2 and **16**, only **17**, sequentially treatment of **15** and **16**.

In vitro internalization on U87-MG cells

The in vitro internalization study performed on U87-MG cells by using [^{123}I]**10** and various amounts of **4** (**Figure 21**). In the results, new method, which was sequentially treated non-labeled RGD peptides, has higher internalized RGD peptides than only [^{123}I]**10** on cancer cell. This results indicated that new strategy may enhance internalization of ligand.

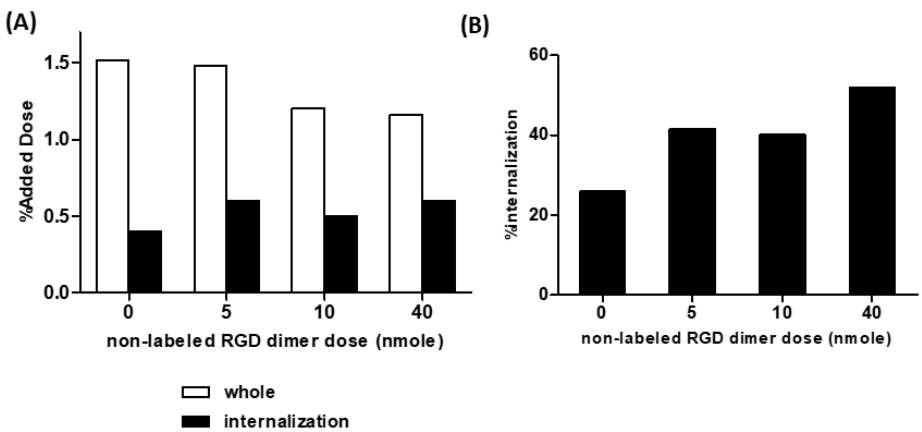

Figure 21. Internalization of RGD peptides in U87-MG cells. (A) %Added dose of [^{123}I]**10** and internalized [^{123}I]**10** with **4** (B) ratio for internalization

5. Ex/In vivo experimental results

Ex vivo biodistribution in tumor xenograft

In ex vivo biodistribution studies, [^{123}I]**10** **(**dimer form**)** or [^{123}I]**11** **(**tetramer form**)** were administered intravenously in U87-MG tumor-bearing nude mice model at four time points (**Figure 22, 23**).

Both [^{123}I]**10** and [^{123}I]**11** were rapidly cleared from blood. The blood levels of two peptides were 0.79% ID/g and 1.77% ID/g at 60 min post-injection, respectively. Rapid and high tumor uptakes of [^{123}I]**10** and [^{123}I]**11** were 14.1 ± 1.59% ID/g and 15.9 ± 1.6% ID/g at 30 min post-injection, respectively. Although in vitro binding affinities for integrin $\alpha_v\beta_3$ were slightly higher in [^{123}I]**11** than in [^{123}I]**10**, there was no significant difference in tumor uptakes between [^{123}I]**10** and [^{123}I]**11**. The tumor uptakes of both RGD peptides decreased to lower than 8.9% ID/g at 2h post-injection.

The [^{123}I]**10** and [^{123}I]**11** have similar clearance kinetics, which passed through renal excretion. The initial renal radioactivity of [^{123}I]**11** (24.2 ± 0.39% ID/g) was two times higher than that of the [^{123}I]**10** (11.6 ± 2.8% ID/g) at 30 min post-injection. Increasing arginine residues, which contains positive charge, may leads to high renal uptakes so that multimeric RGD peptides have major accumulation of radio activities on the renal pathway. Nevertheless, kidney uptakes of both RGD peptides dramatically fell to 8.5 ± 0.6% ID/g and 4.6 ± 0.7% ID/g at 2 h post-injection, respectively.

The accumulation on normal brain was not observed because of low integrin $\alpha_v\beta_3$ expression and an intact blood-brain barrier (BBB). The thyroid uptakes, which caused by the decomposition of RGD peptide to free ^{123}I, was not observed on results of [^{123}I]**10** for 2 h (0.50 ± 0.09% ID/g). In contrast, thyroid uptakes unexpectedly increased at 2 h post-injection with [^{123}I]**11** (3.23 ± 0.59% ID/g).

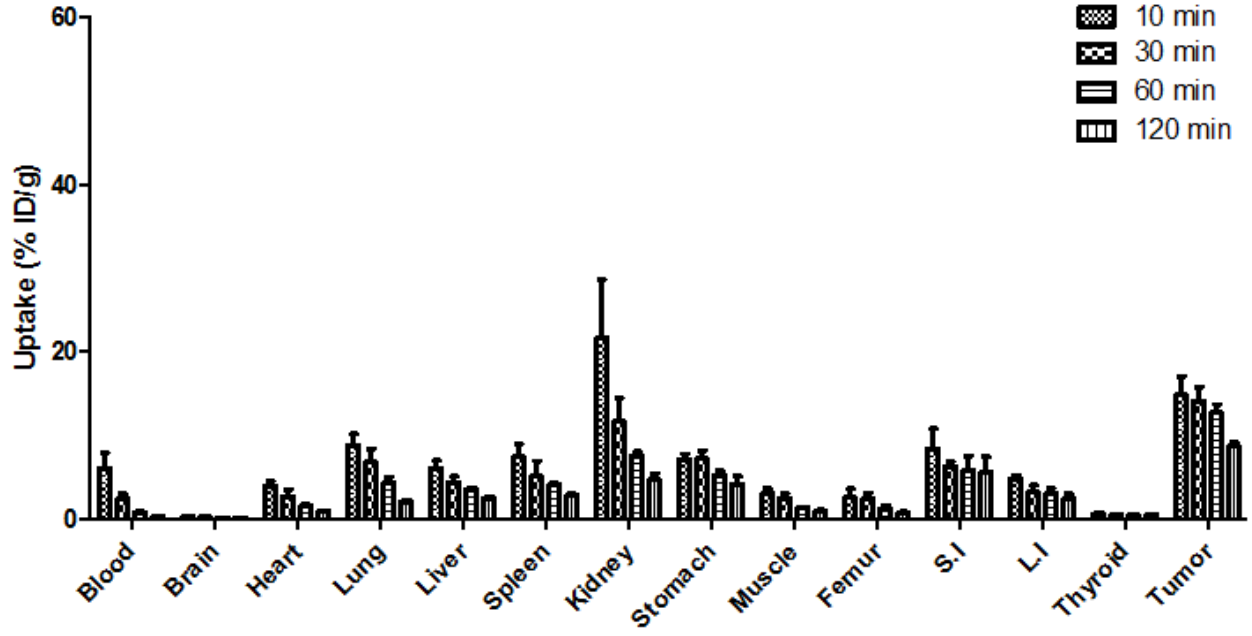

Figure 22. Ex vivo biodistribution of [^{123}I]**10**. Results were expressed as %ID/g; mean ± S.D. (n = 4, each time point). [^{123}I]**10** (0.74 MBq) was injected into U87-MG tumor bearing mice via tail vein.

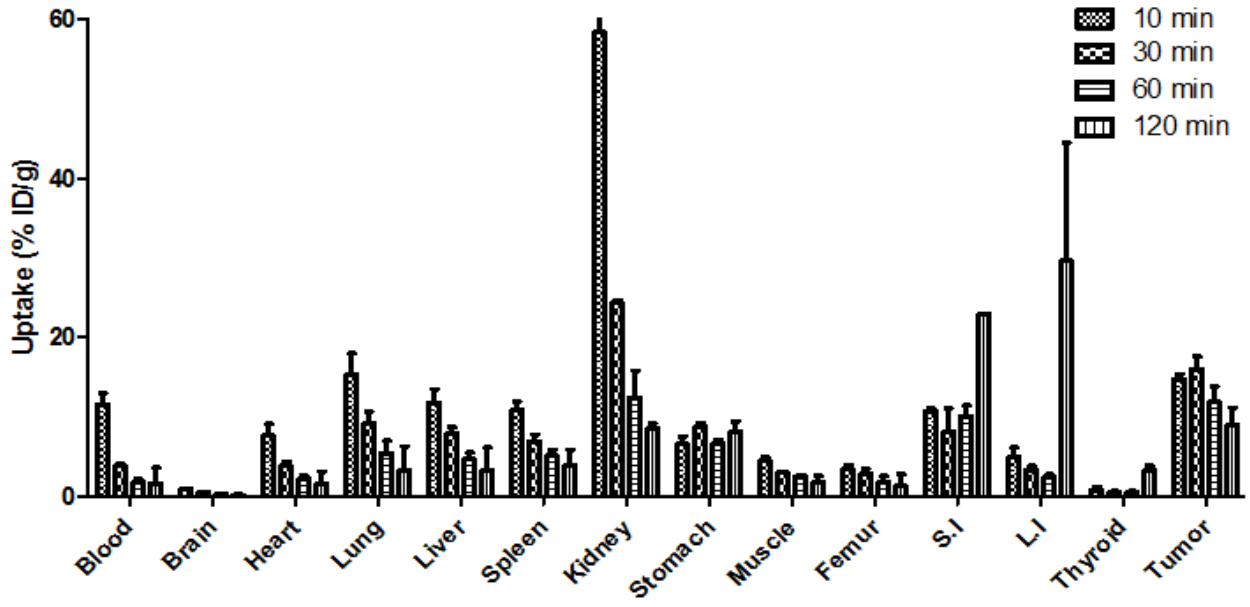

Figure 23. Ex vivo biodistribution of [^{123}I]**11**. Results were expressed as %ID/g; mean ± S.D. (n = 4, each time point). [^{123}I]**11** (0.74 MBq) was injected into U87-MG tumor bearing mice via tail vein.

Small animal SPECT/CT imaging results

[^{123}I]**10** and [^{123}I]**11**

The SPECT/CT imaging of [^{123}I]**10** or [^{123}I]**11** in U87-MG bearing nude mice (*n* = 4, each time point) were performed for 90 min. Quantification of activity accumulation in tumor, kidney, liver and heart was observed (**Figure 24**).

The U87-MG tumor uptake of [^{123}I]**10** and [^{123}I]**11** was similar at 5 min post-injection, which was 13.5 ± 1.3 % ID/g, 13.3 ± 4.1 % ID/g, respectively. The activity accumulation was reached the highest at 5 min post-injection and decreased to almost half in 90 min. Futhermore, similar kinetic and uptakes in liver and heart was observed on both the RGD peptides ([^{123}I]**10** or [^{123}I]**11**).

The SPECT/CT images of both RGD peptides correlated with ex vivo biodistribution data. Positive correlation between ex vivo tumor radioactivity measurements and animal SPECT/CT image analysis (R^2=0.889) was obtained (**Figure 25**). Thus, it appeared that ROI-derived %ID/g values and provide high-confidence values for assessing the angiogenic response in tumor-bearing mice.

Thus, by co-relation with in vivo SPECT/CT images and ex vivo biodistribution data, effect of in vivo intermolecular conjugation (duet bioorthogonal clasp) was determined by in vivo SPECT/CT imaging.

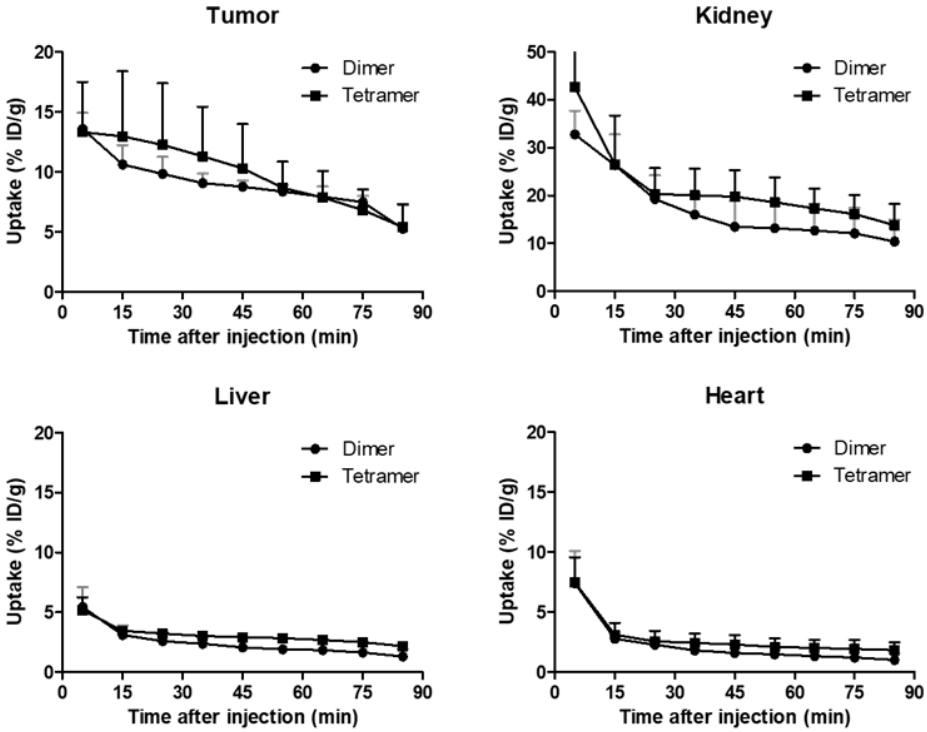

Figure 24. Comparison of small animal SPECT data for [^{123}I]**10** and [^{123}I]**11** Radioactivity of region of interest (ROI) for organs were determined as percentage injected dose per gram (%ID/g). Results are given as the means ± S.D. (n = 4).

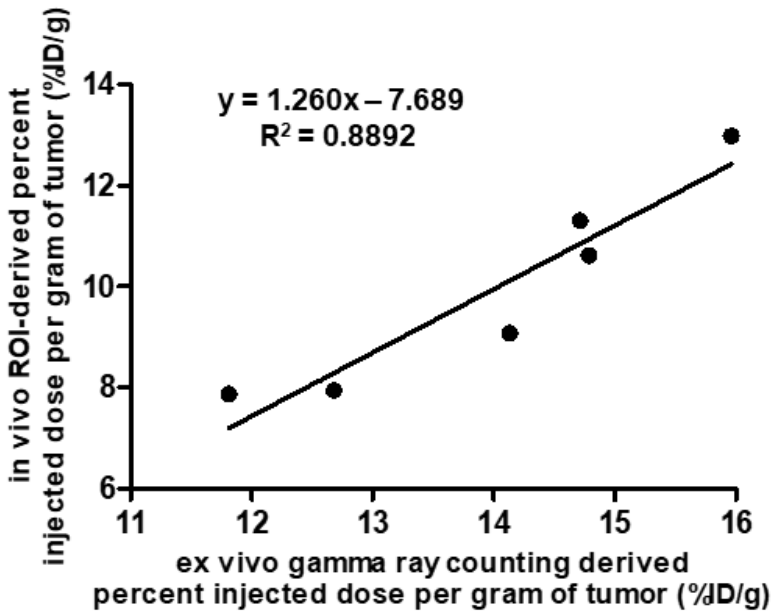

Figure 25. Comparisons of tumor uptake of [^{123}I]**10** and [^{123}I]**11** analyzed by SPECT imaging and dissected biodistribution. Measurement of [^{123}I]**10**, [^{123}I]**11** uptake and calculated tumor activity by in vivo animal SPECT analysis was compared to the true values, as measured ex vivo tumor uptake by gamma counter.

In vivo intermolecular conjugation

The SPECT/CT scans in U87-MG tumor-bearing mouse model were performed to evaluate the effects of in vivo intermolecular conjugation, which named Duet Bioorthogonal Clasp (DBC), with [^{123}I]**10** and **4** (ADIBO-D-[c(RGDfK)]$_2$) for 2 h. Because this strategy included two RGD peptides, which were radioisotope labeled ([^{123}I]**10**) and non-labeled (**4**) RGD peptiedes for sequential injection, two conditions were considered for determining the best condition of this new method (DCB). One was order of ligand injection and the other was amounts of non-labeled ligands.

First, [^{123}I]**10** was injected via the tail vein into the mouse and then three different amounts of **4** was subsequently added after 15 min. Based on a reported pre-targeting study, amounts of non-labeled RGD peptides were selected (18 mg/kg, 1.8 mg/kg, and 0.18 mg/kg) [59].

The initial tumor uptakes for 18 mg/kg, 1.8 mg/kg, and 0.18 mg/kg of **4** (12.4 ± 0.8% ID/g, 11.9 ± 0.9% ID/g, 12.6 ± 0.6% ID/g at 5 min post-injection, respectively) were similar. However, the accumulation of radioactivity at 2 h post-injection. was significantly different (7.47 ± 2.45% ID/g, 7.41 ± 1.92% ID/g, and 9.52 ± 2.1% ID/g, respectively, **Figure 26**). These results suggested that new strategy with the lowest amount (0.18 mg/kg) of peptide **4** t could affect retention time of the RGD peptides at the tumor site for 2 h.

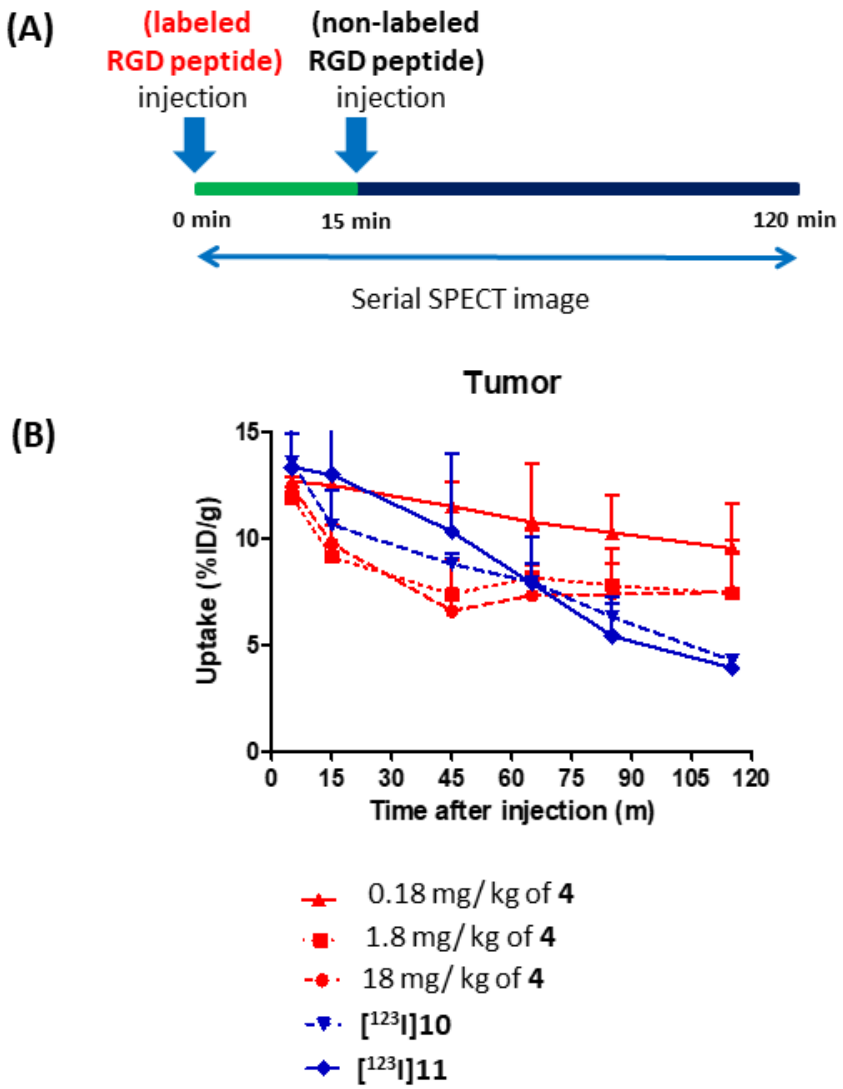

Figure 26. Small animal SPECT/CT images-based measured tumor uptakes. Sequentially injection of [^{123}I]**10** and **4** (18 mg/kg, 1.8 mg/kg, 0.18 mg/kg) for 2 h in U87-MG bearing mouse model. Results are given as the means ± S.D. (n = 3). (A) Protocol of small animal SPECT/CT imaging analysis (B) Comparison of tumor uptakes in different amounts of non-labeled ligand, [^{123}I]**10** and [^{123}I]**11**.

Second, SPECT/CT scans were performed by changing the order of injection, in which non-labeled RGD peptide (18 mg/kg, 1.8 mg/kg, and 0.18 mg/kg) was added first, followed by the injection of **[^{123}I]10**.

The results of SPECT/CT imaging in the tumors were shown in **Figure 27**. Tumor uptakes of different conditions (18 mg/kg, 1.8 mg/kg, and 0.18 mg/kg) have no significant difference between at 15 min (9.30 ± 1.96% ID/g, 9.03 ± 1.72% ID/g, and 9.19 ± 1.31% ID/g, respectively) and at 2 h post injection. (8.45 ± 4.59% ID/g, 8.53 ± 1.99% ID/g, and 6.44 ± 1.30% ID/g).

However, the absolute initial tumor uptake value was lower than that of earlier condition, when the radiolabeled RGD peptide was injected before the non-labeled RGD peptide. This result suggests that the excess non-labeled RGD peptide may act inhibitor to interrupt the binding of radiolabeled RGD peptide to integrin $\alpha_v\beta_3$. In addition, AUC (area under curves) value, which is associated with effect of therapy, was lower than earlier condition.

Thus, from the in vivo imaging studies the best condition for this strategy was determined. The radiolabeled RGD peptide ([^{123}I]**10**) was injected and then subsequently the lowest amount of non-labeled RGD peptide (**4**) for inducing in vivo intermolecular conjugation to prolong retention time of ligand on cancer cells.

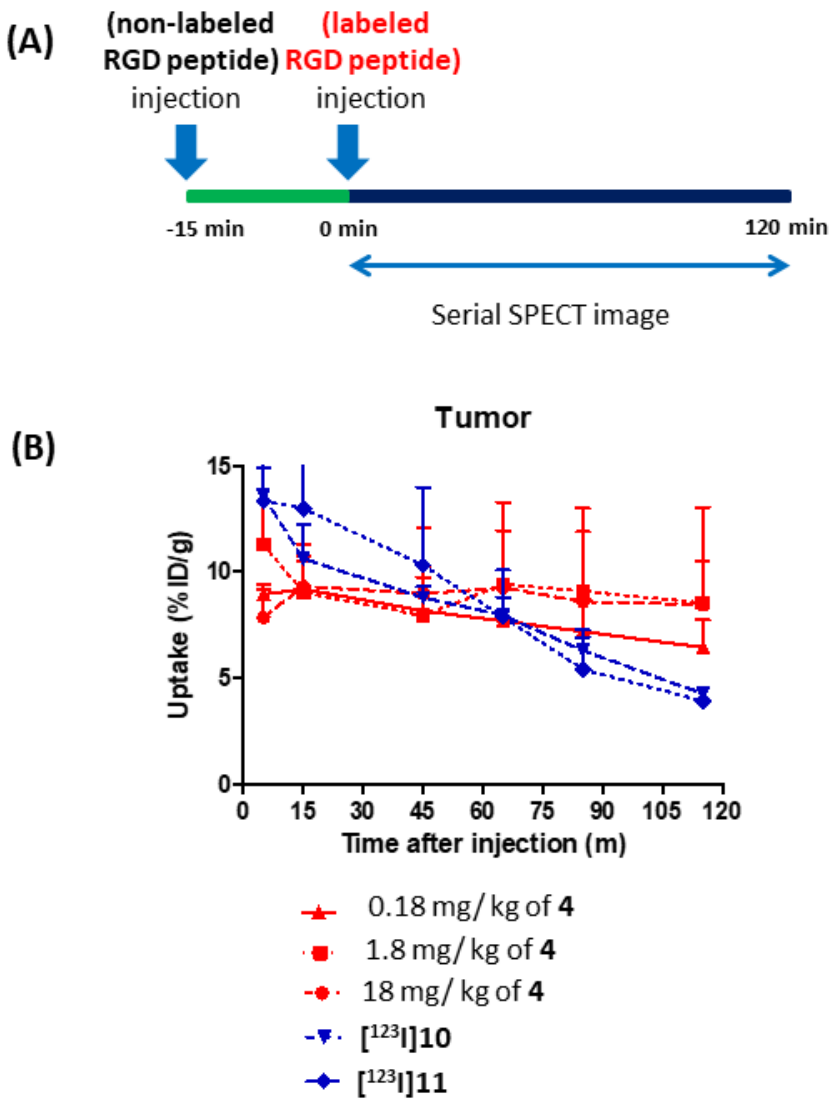

Figure 27. Small animal SPECT/CT images-based measured tumor uptakes. Sequentially injection of **4** (18 mg/kg, 1.8 mg/kg, and 0.18 mg/kg) and [^{123}I]**10** dimer for 120 min in U87-MG xenograft model. Results are given as the means ± S.D. (n = 3). (A) Protocol of small animal SPECT/CT imaging analysis (B) Comparison of tumor uptakes in different amounts of non-labeled ligand, [^{123}I]**10** and [^{123}I]**11**.

To identify the effect of in vivo intermolecular conjugation, the tumor uptakes were compared according to the type of RGD ligand ([^{123}I]**10;** dimer form, [^{123}I]**11;** tetramer form) and the best condition of duet bioorthogonal clasp (sequentially injection of [^{123}I]**10;** dimer form and **4;** dimer form) (**Figure 28**).

The initial tumor uptakes of [^{123}I]**10**, [^{123}I]**11**, and [^{123}I]**10** + **4** were 13.5 ± 1.3% ID/g, 13.3 ± 4.1% ID/g, and 12.6 ± 0.6 % ID/g at 5 min post-injection, respectively. After 85 min of administration, the tumor uptakes of [^{123}I]**10**, [^{123}I]**11** and [^{123}I]**10** + **4** were 5.2 ± 2.1% ID/g, 5.4 ± 1.8 % ID/g, and 10.2 ± 1.7 % ID/g, respectively. In the case of [^{123}I]**10**, [^{123}I]**11**, tumor uptakes significantly decreased for 85 min and remained only 39% and 41% of total radioactivities. However, in vivo intermolecular conjugation (DBC, [^{123}I]**10** + **4**) showed no significant difference in tumor uptakes and remained at over 81% of total radioactivities for 85 min. In addition, half-life of new strategy was 2.5 times higher than that of [^{123}I]**10** and [^{123}I]**11**.

These results suggest that in vivo intermolecular conjugation affected the residence time of RGD peptides indicating stronger and more prolonged binding with integrin $\alpha_v\beta_3$ owing to in vivo click reaction, which conjugated between [^{123}I]**10** and **4**. In addition, these results may be explained by the results of in vitro confocal imaging, which showed that the intermolecular conjugation would induce the internalization into tumor cells. Therefore, this new strategy could lead to improvement in the retention time of RGD peptides and achieve enhanced internalization of multimeric RGD peptides into tumor cells

by forming cluster of ligand bound integrins.

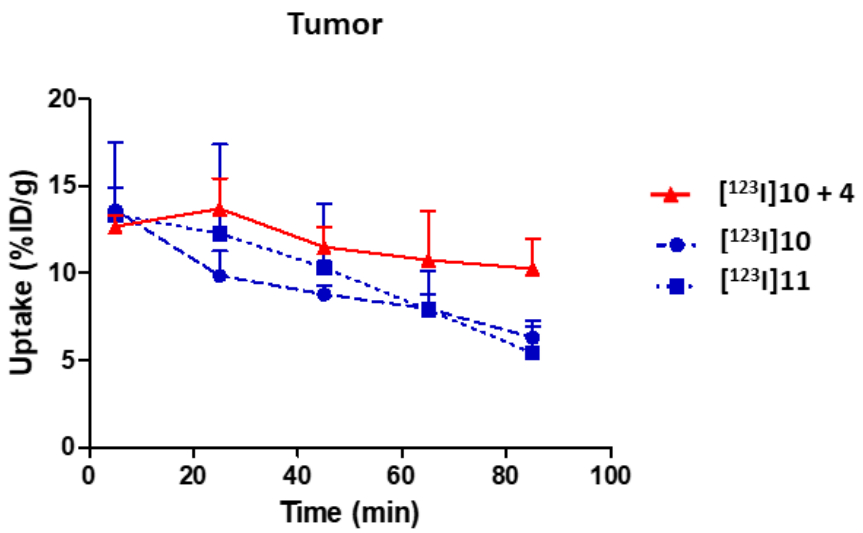

	$T_{½, \beta}$ (min)
[^{123}I]10	82.3
[^{123}I]11	80.7
[^{123}I]10 + 4	213.4

Figure 28. Comparisons of tumor uptake of **[^{123}I]10** and [^{123}I]**11** and [^{123}I]**10 + 4** (DBC). Small animal SPECT/CT images-based measured tumor uptakes for 85 min post-injection in U87-MG tumor bearing mice. (*n* = 3 or 4 for each group). Results are expressed as %ID/g.

As the in vivo intermolecular conjugation induced prolong retention time of RGD peptide, SPECT/CT scans were performed in the U87-MG tumor-bearing mouse model for 24 h. The results are shown in **Figure 29**. The tumor uptake maintained approximately 60% (decay-corrected) for 24 h compared with initial tumor uptake.

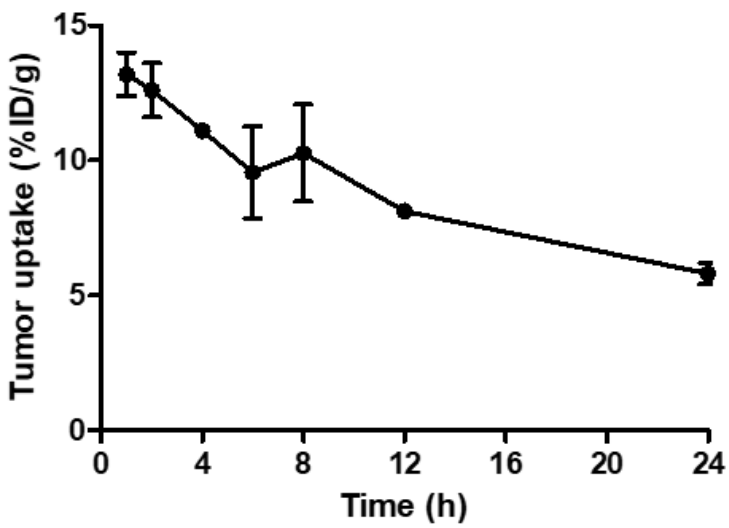

Figure 29. Small animal SPECT/CT images-based measured tumor uptakes by DBC for 24 h. Uptake (decay-corrected) of tumor for 24 h in U87-MG xenografted model (n = 3).

DISCUSSION

The feasibility of in vivo intermolecular conjugation (Duet Bioorthogonal Clasp, DBC) with RGD peptides for angiogenesis targeted therapy was evaluated in the SPECT imaging studies by using U87-MG tumor bearing mouse model.

This study describs the synthesis and radiosynthesis of different RGD peptide dimers which are available in vivo intermolecular conjugation using Click reaction. In addition, different RGD peptide dimers, which contain pairs for Click reaction, are easily modified as fluorescent imaing probe as well as SPECT radiotracer. The prepared RGD peptides, [^{123}I]**10** (dimer form) and [^{123}I]**11** (tetramer form), had a high binding affinity for integrin $\alpha_v\beta_3$ as determined by competitive cell-binding assay. Then, the in vivo binding affinity and specificity of [^{123}I]**10** and [^{123}I]**11** was also confirmed by ex vivo biodistribution studies and small animal SPECT/CT scans.

Although radiolabeled RGD peptides has been developed for tumor therapy, RGD-based tracers washed out rapidly from the tumor site because of possibly inadequate binding with integrin $\alpha_v\beta_3$ under in vivo environment. This challenge has limited the application of targeted cancer therapy.

DBC, which induced intermolecular conjugation by an sequential injection of RGD peptides, was investigated by using FRET analysis and SPECT/CT imaging for strong binding between integrin $\alpha_v\beta_3$. The

results of in vitro FRET analysis indicated that this strategy has the potential for inducing internalization into the cancer cell. Fluorescence signals by intermolecular conjugation were localized in inside U87-MG cells.

For measuring tumor uptake, in vivo SPECT/CT imaging studies on different amounts of non-labeled RGD peptide and the change of injection order were carried out to optimize condition for in vivo intermolecular conjugation was established. Moreover, non-radiolabeled RGD peptide may act as a blocker that interrupted the binding of radiolabeled RGD peptide to integrin $\alpha_v\beta_3$. The usage of the lowest amounts of non-labeled RGD peptide and later injection could prolong the retention time of ligand on the tumor.

In the comparison of tumor uptake between [^{123}I]**11** (tetramer form) and DBC, the RGD peptides remained at target site for longer for 2 h by new strategy. This result suggests that tetramer form, prepared by in vitro click reaction, was not enough for simultaneous binding to adjacent four integrin $\alpha_v\beta_3$. In the contrast, this strategy may lead to binding of all RGD peptide for integrin $\alpha_v\beta_3$ via intermolecular conjugation and to induce internalization into tumor cells by clustering of integrins via strong conjugation of ligands.

These results suggest that this method can pave the way to various successful application such as targeted radionuclide therapy, therapeutic drug delivery, targeted photodynamic therapy, and imaging guided surgery.

CONCLUSION

In this study, a new in vivo intermolecular conjugation-based strategy was demonstrated to induce internalization of RGD peptides into cancer cells more efficiently.

The RGD peptides for in vivo intermolecular conjugation were successfully synthesized and labeled with fluorescent dyes or radioisotopes. In vitro FRET analysis using confocal microscopy suggested that new method induced internalization of RGD peptides into the cancer cells. The results of in vivo and ex vivo studies with iodine-123 labeled RGD peptides indicated that tumor uptake was maintained for 24 h by new method.

Thus, this new strategy could be used as a promising tool not only for anti-angiogenic radiotherapy, but also for enhancing drug delivery, in general.

[APPENDIX 1] Radioiodo-labeled RGD peptides

Iodine is an ideal radioisotope for nuclear medicine diagnostics and therapy. ^{131}I is suitable for therapeutic radionuclide, which has short range beta radiation (971 keV) and also emitted gamma ray, has adequate the half-life time (8.06 days) for therapeutic treatments [1]. In addition, iodination of biomolecules is well established.

^{123}I is usually produced by cyclotron from bombardment of antimony-121 or tellurium-122 or –124 and has been used for diagnostics due to emit only gamma ray [2]. The half-life time (13.2 h) sufficiently long to measure biokinetics for diagnosis. In addition, ^{131}I is used for radionuclide therapy as converting ^{123}I to ^{131}I without modifying precursors [3]. For these properties, ^{123}I and ^{131}I are “matched pairs” for theranostics, which is useful radioisotopes for in vivo imaging and therapy, respectively.

References [1] Mandel S.J., Shankar L.K., Benard F., Yamamoto A., Alavi A. Superiority of Iodine-123 Compared with Iodine-131 scanning for thyroid remnants in patients with differentiated thyroid cancer. *Clin Nucl Med.* 2001;26:6. [2] Buscombe J.R. Radionuclides in the management of thyroid cancer. *Cancer Imaging.* 2007;7:202.[3] Yordanova A., Eppard E., Kürpig S., Bundschuh R.A., Schönberger., Gonzalez-Carmona M., Feldmann G., Ahmadzadehfar H., Essler M. Theranostics in nuclear medicine practice. *Onco Targets Ther.* 2017;10:4821.

[APPENDIX 2] FRET microscopy

Fluorescence resonance energy transfer (FRET) is a photophysical phenomenon, which relies on distance dependent transfer of energy between donor and acceptor fluorophores [1]. Conformational dynamic and interactions of biomolecules is observed in real time by measuring FRET signals [2]. Donor fluorophore is excited by external light and energy of excited state transferred to acceptor fluorophore [3]. This leads to reduce donor's fluorescence intensity and to increase acceptor's emission intensity. Fluorescence signals by transference of energies depend on distances between donor and acceptor. This technique is useful to evaluate changes in nanometer scale distances. Several pairs of fluorescence dyes, which have large spectral separation between donor and acceptor emissions, are used for FRET [4]. Among small organic dyes, fluorescein isothiocyanate (FITC) and tetramethylrhodamin (TRITC) are also suitable pairs for FRET analysis. Two fluorescence dyes have proper spectrums for transferring energies from donor to acceptor [5]. The selected dyes show absorption and emission spectra overlap for transferring energies from emission of the donor to excitation of the acceptor. In this study, we selected pairs (FITC and TRITC) of small organic dyes to evaluate conjugation between RGD dimers by click reaction.

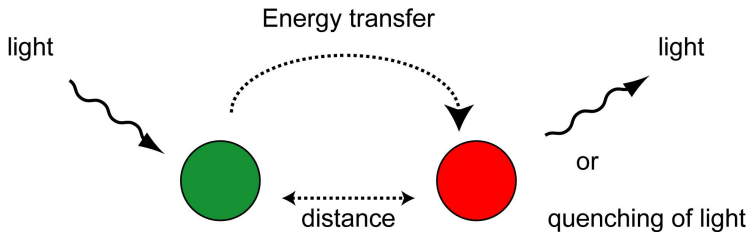

Diagram of fluorescence resonance energy transfer (FRET) [3].

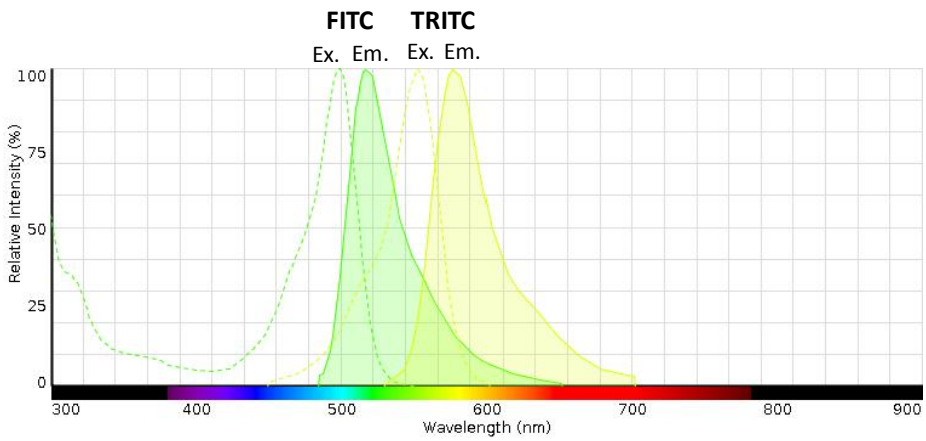

Excitation (Ex.) and emission (Em.) spectra of FITC and TRITC. The FITC emission spectrum overlaps the TRITC excitation spectrum for FRET

References [1] Selvin P.R. The renaissance of fluorescence resonance energy transfer. *Nat Struct Biol.* 2000;7:730. [2] Yamauchi F., Kamioka Y., Yano T., Matsuda M. In vivo FRET imaging of tumor endothelial cells highlights a role of low PKA activity in vascular hyperpermeability. *Cancer Res.* 2016;76:5266. [3] Van der Wal S., de Korne C.M., Sand L.G.L. Bioorthogonally Applicable Fluorescence Deactivation Strategy for Receptor Kinetics Study and Theranostic Pretargeting Approaches. *ChemBioChem.* 2018;19:1758. [4] 1. Lleress D., Swift S., Lamond A.I. Detecting Protein-Protein Interactions In Vivo with FRET using Multiphoton Fluorescence Lifetime Imaging Microscopy (FLIM). *Curr Protoc Cytom.* 2007:1. [5] Fehr M., Lalonde S., Lager I., Wolff M.W., Frommer WB. In vivo imaging of the dynamics of glucose uptake in the cytosol of COS-7 cells by fluorescent nanosensors. *J Biol Chem.* 2003;278:19127.

REFERENCES

1. Torre L.A., Bray F., Siegel R.L., Ferlay J., Lortet-Tieulent J., Jemal A. Global cancer statistics, 2012. *CA Cancer J Clin*. 2015;65:87.

2. Falzone L., Salomone S., Libra M. Evolution of cancer pharmacological treatments at the turn of the third millennium. *Front Pharmacol*. 2018;9:1.

3. Wu H.C., Chang D.K., Huang C.T. Targeted therapy for cancer. *J Cancer Mol.* 2006;2:57.

4. MacDonald V. Chemotherapy: Managing side effects and safe handling. *Can. Vet. J.* 2009;50:665-668.

5. Bruce. A.C, Thomas G.R. Chemotherapy and the war on cancer. *Nat Rev Cancer*. 2005;5:65.

6. Gerber D.E. Targeted therapies: a new generation of cancer treatments. *Am Fam Physician*. 2008;77:311.

7. Chon H.S., Hu W., Kavanagh J.J. Targeted therapies in gynecologic cancers. *Curr. Cancer Drug Targets.* 2006;6:333-363.

8. Yan L., Rosen N., Arteaga C. Editorial Challenges in Targeted Cancer Drug Development. *Chinese Anti-Cancer Assoc.* 2011;31:1.

9. Olivo M., Bhuvaneswari R., Lucky S.S., Dendukuri N., Thong P.S.P. Targeted therapy of cancer using photodynamic therapy in combination with multi-faceted anti-tumor modalities. *Pharmaceuticals*. 2010;3:1507-1529.

10. Bae Y.H., Park K. Targeted drug delivery to tumors: Myths, reality, possibility. *J Control Release.* 2012;153:198.

11. Srinivasarao M., Galliford C.V., Low P.S. Principles in the design of ligand-targeted cancer therapeutics and imaging agents. *Nat. Rev. Drug Discov.* 2015;14:203-219.

12. Wu L. Qu X. Cancer biomarker detection: recent achievements and challenges. *Chem. Soc. Rev.* 2015;44:2963-2997.

13. Falco M., Palma G., Rea D., De Biase D., Scala S., D'Aiuto M., Facchini G., Perdonà S., Barbieri A., Arra C. Tumour biomarkers: homeostasis as a novel prognostic indicator. *Open Biol.* 2016;6: 160254.

14. Hanahan D., Weinberg R.A. Hallmarks of cancer: the next generation. *Cell*. 2011;144:646.

15. Danhier F., Breton A.L., Preat V. RGD-based strategies to target alpha(v) beta(3) integrin in cancer therapy and diagnosis. *Mol Pharmaceutics.* 2012;9:2961−2973.

16. Gupta M.K., Qin R.Y. Mechanism and its regulation of tumor-induced angiogenesis. *World. J. Gastroenterol.* 2003;9:1144-1155.

17. Mahabeleshwar G.H., Feng W., Reddy K., Plow E.F., Byzova T.V. Mechanisms of integrin – Vascular endothelial growth factor receptor cross-activation in angiogenesis *Circ Res.* 2007;101:570-580.

18. Lawson C. Schlaepfer DD. Integrin adhesions: Who's on first?

What's on second?. *Cell Adh Migr.* 2012;6:302-306.

19. Liu Z., Wang F., Chen X. Integrin $\alpha_v\beta_3$-targeted cancer therapy. *Drug Develop Res.* 2008;69:329-339.

20. Loizzi V, del Vecchio V, Gargano G, et al. Biological pathways involved in tumor angiogenesis and bevacizumab based anti-angiogenic therapy with special references to ovarian cancer. *Int J Mol Sci.* 2017;18:1.

21. Desgrosellier J.S., Cheresh D.A. Integrins in cancer: biological implications and therapeutic opportunities. *Nat Rev Cancer.* 2010;10:9.

22. Liu Z., Wang F., Chen X. Integrin $\alpha_v\beta_3$-Targeted Cancer Therapy. *Drug Dev Res.* 2008; 69: 329-339.

23. Beer A.J., Kessler H., Wester H.J. Schwaiger M. PET Imaging of Integrin $\alpha_v\beta_3$ Expression. *Theranostics.* 2011;1:48–57.

24. Ruoslahti E. RGD and other recognition sequences for integrins. *Annu Rev Cell Dev Biol.* 1996;12:697-715.

25. Ruoslahti E., Pierschbacher M.D. Arg-Gly-Asp: a versatile cell recognition signal. *Cell.* 1986;44:517-518.

26. Bogdanowich-Knipp S.J., Chakrabarti S., Williams T.D., Dillman R.K., Siahaan T.J. Solution stability of linear vs. cyclic RGD peptides. *J. Pept. Res.* 1999;53:530-41.

27. Suna X., Lia Y., Liua T., Lia Z., Zhanga X., Chen X. Peptide-based imaging agents for cancer detection. *Adv. Drug. Deliv. Rev.* 2017;110-111:38-51.

28. Haubner R., Gratias R., Diefenbach B., Goodman S.L., Jonczyk A., Kessler H. Structural and functional aspect of RGD-containing cyclic pentapeptides as highly potent and selective integrin $\alpha_v\beta_3$ antagonists. *J Am Chem Soc.* 1996;118:7461-7472.

29. Aumailley M., Gurrath M., Mu¨ller G., Calvete J., Timpl R., Kessler H. Arg-Gly-Asp constrained within cyclic pentapeptides strong and selective inhibitors of cell adhension to vitronectin and laminin fragment P1. *FEBS Lett.* 1991;291:50-54.

30. Zhou Y., Chakraborty S., Liu S. Radiolabeled cyclic RGD peptides as radiotracers for imaging tumors and thrombosis by SPECT. *Theranostics.* 2011;18:58-82.

31. Liu S. Radiolabeled multimeric cyclic RGD peptides as integrin α_v β_3 targeted radiotracers for tumor imaging. *Mol Pharmaceut*. 2006;3:472-487.

32. Lucie S., Elisabeth G., Stéphanie F., Guy S., Amandine H., Corinne A.R., Didier B., Catherine S., Alexeï G., Pascal D., Jean-Luc C. Clustering and internalization of integrin $\alpha_v\beta_3$ with a tetrameric RGD-synthetic peptide. *Mol Ther*. 2009;17:837–843.

33. Beer A.J., Kessler H., Wester H.J., Schwaiger M. PET imaging of integrin $\alpha_v\beta_3$ expression. *Theranostics.* 2011;1: 48-57.

34. Bridgewater R.E., Norman J.C., Caswell P.T. Integrin trafficking at a glance. *J. Cell Sci.* 2012;125:3695-3701.

35. Franceschi N.D., Hamidi H., Alanko J., Sahgal P., Ivaska J. Integrin traffic – the update. *J. Cell Sci.* 2015;128:839-852.

36. Paul N.R., Jacquemet G., Caswell P.T. Endocytic trafficking of integrins in cell migration. *Curr. Biol.* 2015;25:R1092-R1105.

37. Yu C.H., Rafiq N.B.M, Cao F., Zhou Y., Krishnasamy A., Biswas K.H., Ravasio A., Chen Z., Wang Y.H., Kawauchi K., Jones G.E., Sheetz M.P. Integrin-beta3 clusters recruit clathrin-mediated endocytic machinery in the absence of traction force. *Nat Commun.* 2015;6: 8672.

38. Changede R., Sheetz M. Integrin and cadherin clusters: A robust way to organize adhesions for cell mechanics. *Bioessays.* 2017;39:1-12.

39. Srichai M., Zent R. 2010. Integrin structure and function. In Zent R., Pozzi A. (Eds), Cell-extracellular matrix interactions in cancer. (pp.19-41). New York, NY; Springer.

40. Gestwicki J.E., Cairo C.W., Strong L.E., Oetjen K.A. Kiessling L.L. Influencing receptor-ligand binding mechanisms with multivalent ligand architecture. *J. Am. Chem. Soc.* 2002;124: 14922-14933.

41. Castel S., Pagan R., Mitjans F., Piulats J., Goodman S., Jonczyk A. Huber F., Vilarò S., Reina M. RGD peptides and monoclonal antibodies, antagonists of αv-integrin, enter the cells by independent endocytic pathways. *Lab. Invest.* 2001;81:1615-1626.

42. Schraa A.J., Kok R.J., Berendsen A.D., Moorlag H.E., Bos E.J., Meijer D.K., de Leij L.F., Molema G. Endothelial cells internalize and degrade RGD-modified proteins developed for tumor vasculature targeting. *J. Control. Release.* 2002;83:241-251.

43. Wu Z., Li Z.B., Chen K., Cai W., He L., Chin F.T., Li F., Chen X. microPET of Tumor Integrin $\alpha_v\beta_3$ Expression Using ^{18}F-Labeled PEGylated Tetrameric RGD Peptide (^{18}F-FPRGD4). J *Nucl Med.* 2007;48:1536.

44. Lee B.C., Moon B.S., Kim J.S., Jung J.H., Park H.S., Katzenellenbogen J.A. Kim S.E. Synthesis and biological evaluation of RGD peptides with the ^{99m}Tc/^{188}Re chelated iminodiacetate core: highly enhanced uptake and excretion kinetics of theranostics against tumor angiogenesis. *RSC. Adv.* 2013;3:782-792.

45. Janssen M.L., Oyen W.J., Dijkgraaf I., Massuger L.F., Frielink C., Edwards D.S., Rajopadhye M., Boonstra H., Corstens F.H., Boerman O.C. Tumor targeting with radiolabeled $\alpha_v\beta_3$ integrin binding peptides in a nude mouse model. *Cancer Res.* 2002;62:6146–6151.

46. Liu Z., Shi J., Jia B., Yu Z., Liu Y., Zhao H., Li F., Tian J., Chen X., Liu S., Wang F. Two ^{90}Y-Labeled multimeric RGD peptides RGD4 and 3PRGD2 for integrin targeted radionuclide therapy. *Mol. Pharmaceutics.* 2011;8:591-599.

47. Shi J, Wang F, Liu S. Radiolabeled cyclic RGD peptides as radiotracers for tumor imaging. *Biophys Reports*. 2016;2:1.

48. Liu S. Radiolabeled Cyclic RGD Peptide Bioconjugates as Radiotracers Targeting Multiple Integrins. *Bioconjug Chem*. 2015;26:1413.

49. Kolb H.C., Finn M.G., Sharpless K.B. Click chemistry: diverse chemical function from a few good reactions. *Angew Chem Int Ed*

Engl. 2001;40:2004-2021.

50. Moses J.E., Moorhouse A.D. The growing applications of click chemistry. *Chem Soc Rev.* 2007;36:1249-1262.

51. Jang S., Sachin K., Lee H.J., Kim D.W., Lee H.S. Development of a simple method for protein conjugation by copper-free click reaction and its application to antibody-free Western blot analysis. *Bioconjug Chem.* 2012;23:2256-2261.

52. Baskin J.M., Prescher J.A., Laughlin S.T., Agard N.J., Chang P.V., Miller I.A., Lo A., Codelli J.A., Bertozzi C.R. Copper-free click chemistry for dynamic in vivo imaging. *Proc Natl Acad Sci USA.* 2007;104:16793.

53. Codelli J.A., Baskin J.M., Agard N.J., Bertozzi C.R. Second-generation difluorinated cyclooctynes for copper-free click chemistry. *J. Am. Chem. Soc.* 2008;130:11486-11493.

54. Bouvet V., Wuest M., Wuest F. Copper-free click chemistry with the short-lived positron emitter fluorine-18. *Org. Biomol. Chem.* 2011;9:7393-7399.

55. Blackman M.L., Royzen M., Fox J.M. Tetrazine Ligation: fast bioconjugation based on inverse-electron-demand Diels-Alder reactivity. *J. Am. Chem. Soc.* 2008;130:13518-135189.

56. Jewetta J.C., Bertozzi C.R. Cu-free click cycloaddition reactions in chemical biology. *Chem. Soc. Rev.* 2010;39:1272-1279.

57. Hein C.D., Liu X.M., Wang D. Click chemistry, a powerful tool for pharmaceutical sciences. *Pharm. Res.* 2008;25:2216-2230.

58. Schottelius M., Konrad M., Osl T., Poschenrieder A., Wester H.J. An optimized strategy for the mild and efficient solution phase iodination of tyrosine residues in bioactive peptides. *Tetrahedron Lett.* 2015;56:6602–6605.

59. Lee S.B., Kim H.L., Jeong H.J., Lim S.T., Sohn M.H., Kim D.W. Mesoporous silica nanoparticle pretargeting for PET imaging based on a rapid bioorthogonal reaction in a living body. *Angew Chem Int Ed.* 2013;52:10549–10552.

국 문 초 록

종양 표적 치료는 기존의 항암제, 수술적 접근 또는 외부 방사선조사를 이용한 방법과는 달리 종양의 특이적 활성에 관여하는 바이오마커만을 표적으로 하는 치료 방법이다. 현재까지 알려진 종양 표적 치료 방법으로는 표적항암제 치료, 방사성동위원소 치료, 광역학 치료 같은 방법이 있으며 모두 종양세포의 사멸과 함께 정상 세포의 손상을 최소화하는 목적을 지니고 있다. 이 치료에 사용되는 약물이나 펩티드 또는 단백질은 종양 특이 바이오마커에 높은 결합능과 정상 장기에는 낮은 분포 그리고 종양에 높은 머무름을 가져야 하며, 종양세포 내로 세포 내재화(internalization)가 요구된다.

본 연구에서는 종양에 발현되는 하나의 특이적 수용체를 표적하는 서로 다른 펩티드를 순차적으로 주입 후, 수용체에 결합된 펩티드들 간에 체내 분자 간 결합 반응을 유도하는 방법(Duet Bioorthogonal Clasp)을 고안하였다. 이 방법은 종양 주변에 분포하는 수용체에 자리 잡은 펩티드 간의 체내 분자 간 결합으로 수용체들 사이에 복합결합체(cluster)를 형성시키고 기존의 표적 수용체와 펩티드 혼합체가 종양 세포 내부로 이동되는 현상

(endocytosis)을 유도하여 주입한 펩티드의 종양세포 내 머무름을 증진시켜 표적 치료 효과를 향상시키는 목적이 있다. 이를 위해 종양 특이 바이오마커로 종양 신생혈관생성에 연관되어있고 종양 근처 혈관에 존재하는 인테그린 $\alpha_v\beta_3$ 수용체를 선택하였고 이에 높은 결합력을 갖는 RGD 펩티드들을 리간드로 합성하였다. 서로 다른 두 펩티드의 체외 종양 세포에서 이동 및 분포를 확인하고자 형광영상이 가능한 형광 염료 (FITC 또는 TRITC)가 도입된 RGD 펩티드를 합성하였으며, 체내 종양에서 분포를 확인하고자 단일광 전자단층촬영(SPECT) 영상 획득을 위해 펩티드 잔기의 타이로신에 방사성동위원소(^{123}I 또는 ^{125}I)를 표지하였다.

새로 고안한 방법인 두 개의 서로 다른 RGD 펩티드로 체내 분자 간 결합을 유도 하였을 때, 종양 세포 내로 이동하는 정도가 현격히 증가됨을 FRET 형광 영상분석을 통해 확인하였다. 방사성 요오드가 도입된 RGD 펩티드를 이용한 체내 SPECT/CT 영상에서도 하나의 RGD 펩티드는 2시간 후 종양에 39%가 남아있는 것에 비해, 본 연구의 방법은 81%로 종양 섭취가 남아 있음을 확인하였으며 24 시간 동안에도 60%의 종양 섭취가 유지되고 있음을 확인하였다.

본 연구에서 종양 표적 치료를 위해 고안된 방법은 종양 근처의

수용체 간 복합결합체를 형성을 도와 리간드의 종양 세포 내재화 촉진을 유도하는 방법임을 확인하였으며 향후에 종양의 방사성동위원소치료 및 항암약물 전달 방법과 같은 다양한 종양표적치료에 이용이 확대될 것으로 기대한다.

주요어 : 표적 종양 치료, 세포 내 이입, 신생혈관, RGD 펩타이드, 복합결합체

학 번 : 2014-30819